Risk-Hedged Traffic Flow Management under Airspace Capacity Uncertainties

Prasenjit Sengupta[*], Monish D. Tandale[†], and P. K. Menon[‡]
Optimal Synthesis Inc., Los Altos, CA 94022-2777

This paper presents a novel solution to the problem of air traffic flow management under airspace capacity uncertainty arising from weather or environmental effects. The traffic flow management problem is formulated as a stochastic Linear Program with multiple available routes between origin-destination pairs, with the weather/environmental factors constraining the probable capacities along these routes. The performance index consists of the delays introduced by deterministic and stochastic capacity constraints. Primary impact of the weather/environmental factors is to require the rerouting of aircraft, causing additional delays. These additional delays require the aircraft to carry additional fuel or to incur costs associated with the failure to meet the schedules in hub-spoke operations. Thus, the variance of delays can be used to define the degree of risk in stochastic traffic flow management, and flow management algorithms that assure the variations in the delay below a specified value can be considered as providing a hedge against uncertain weather or environmental factors. The algorithm developed in this paper produces a risk-hedged decision that results in the least delay at a specified level of acceptable variance. This algorithm represents a dramatic departure from the more traditional stochastic traffic flow management algorithms which minimize expected value of delays, without attempting to control their variances. The performance of the present stochastic traffic flow management algorithm is demonstrated on a Use Case representing National Airspace System operations on a regional scale.

I. Introduction

The impact of stochastic airspace capacity on the National Airspace System (NAS) is a well-studied phenomenon. Uncertainty in airspace capacity originates in the unpredictability associated with atmospheric hazards

[*] Research Scientist, 95 First Street Suite 240, Senior Member AIAA.
[†] Senior Research Scientist, 95 First Street Suite 240, Senior Member AIAA.
[‡] Chief Scientist and President, 95 First Street Suite 240, Fellow AIAA.

or climate disruptions, which refer to any phenomenon that adversely impacts NAS capacity and its ability to perform efficiently. Examples include volcanic ash, which is an infrequent problem, but can make large areas of the airspace unavailable, or weather events, which are more frequent, but a localized problem. By some estimates [1,2], the eruption of the Eyjafjallajökull volcano in Iceland resulted in a loss of $200 million a day for the worldwide aviation industry, and totaled $1.7 billion over the duration of the emission of ashes into the atmosphere. Further losses to trade, due to logistical issues, were not accounted for in these studies. A detailed study of the impact of volcanic ash hazard on the performance and delays in the National Airspace System (NAS) is given in [3]. Although the immediate impact of an atmospheric hazard is on the capacity of the enroute airspace, in some cases, airports or terminal area operations can also be affected. For instance, portions of the airspace are inaccessible due to the potential damage that volcanic ash can cause on aircraft components [4]. Similarly, fog, or marine stratus, is a known problem at San Francisco International Airport affecting the Airport Acceptance Rate and Airport Departure Rate (AAR and ADR respectively) at the airport. Adverse weather can also affect capacity indirectly through an increase in controller workload, possibility of airport closure, and congestion on the airport surface [3].

Efforts have been made to model the disruption in NAS operations due to many atmospheric hazards, and statistical studies of the NAS have been performed with these models [6-7]. If trajectories of all flights and the future capacity of the NAS resources are known exactly, then traffic flow management (TFM) performed is deterministic in nature. Deterministic TFM is well understood [8-21], and computationally feasible algorithms are known that can manage NAS traffic while minimizing overall system delay. Under many circumstances, deterministic TFM models cannot accommodate demand (traffic) and capacity uncertainty, resulting in increased delays and conflicts in schedule. Such situations are explored in [22], where a study evaluated the robustness of a deterministic TFM algorithm, viz. the Bertsimas-Stock Patterson (BSP) model [23,24], in the presence of uncertainty.

Deterministic TFM optimization methods such as the BSP model obtain TFM directives (e.g. ground hold and airborne delays), but once these directives are incorporated in flight's schedule, the efficiency of operations in the NAS can be ascertained *a priori*. However, variability in demand and capacity due to extraneous factors can cause deviation from the nominal performance and result in additional delays.

This paper presents a novel stochastic TFM algorithm that can manage traffic in the presence of uncertainties. In this work, uncertainty in capacity is stressed upon, mirroring the prevalent opinion that one of the major challenges in future TFM will the ability "to make good decisions in the presence of uncertainty in the prediction of weather" [25]. Results can be extended to address demand uncertainty formulations [26-33]. However, demand uncertainty is beyond the scope of this paper.

To motivate the relationship between stochastic weather phenomena and the stochastic TFM, consider Figure 1, which shows probabilistic thunderstorm forecasts from the National Oceanic and Atmospheric Administration (NOAA), in terms of confidence curves. It is evident that to a route which completely avoids any possible interaction with weather, e.g. the 10%, threshold may require an unreasonably long route. More importantly, even within the region of high probability (where 'high' is a set threshold, say 70%), weather is essentially probabilistic, and can be represented by a set of weather realizations, with associated probability values.

A schematic diagram showing three weather scenarios is shown in Figure 2. Each scenario has an associated probability p_i and interacts with the nominal route of an aircraft flying between a given origin / destination pair. The weather phenomena are depicted by solid, dashed, and dotted curves.

When a weather scenario is realized, the flight will likely have to modify its route in response to the weather. Therefore, a number of reroutes can be calculated, starting from the end of the common trajectory, which an aircraft flies before any knowledge of the specific weather instance is available (although the statistical data may be available). The reroutes in response to weather are shown as solid, dashed, and dotted trajectories in Figure 3.

Depending on which weather scenario is ultimately realized, the flight will follow one of the trajectories. Since trajectories are generally of different length, this causes the entry time of the flight into a downstream Sector to be a stochastic quantity, and consequently, the arrival time at the destination airport is also a stochastic quantity whose stochasticity is linked to the probabilistic behavior of weather. The sample flight times for each scenario are shown as the values *t1*, *t2*, and *t3* in this figure. A strategy which seeks to minimize the expected value of delay without any consideration of the variance is known as a *risk-neutral* strategy.

It is possible to follow other strategies. For instance, Figure 4 depicts an intermediate strategy where the flight follows the same weather avoidance route for two scenarios (depicted as the solid line), and a different route for the third scenario, depicted by the dashed line. Since the route flown in response to the first two scenarios is longer than the route flown in response to the first scenario in the risk-neutral strategy, the expected value of the delay time increases as shown at the top of Figure 4, but the variation in the delay from the mean decreases. An extreme strategy is shown in Figure 5, where the flight follows the indicated reroute regardless of which weather scenario is realized, because this route avoids all simulated scenarios. However, the flight time using this route is the largest among the three. Using this *risk-averse* strategy, the expected delay is the largest; however, the variance is zero.

The relationship between expected delay, variation in delay, and choice of strategy motivates a multi-objective tradeoff. Multi-objective problems that balance mean throughput against variance are common in financial engineering [34], where the mean throughput is interpreted as the expected return-on-investment of a portfolio, and the variance is interpreted as the associated risk. A portfolio in the context of financial engineering is a convex combination of resources with known return and risk, where the decision variables are the proportions with which each resource is selected.

Stochastic TFM with an aim to maximize mean throughput or to minimize mean delays are alone not sufficient for probabilistic TFM. Recent works in the literature [35-39] have addressed the issue of minimizing the expected value of delays using either an LP framework or flow-based optimization. Stochastic Linear Programming has also been used by Clare and Richards [40] to obtain TFM solutions with probabilistic capacity constraints, although [40] allows for capacity violations, and does not address the resulting variability in performance.

The authors believe that the work presented in this paper is the first to address the management of variance in addition to delay minimization TFM. This is an important result, because – as noted earlier – NAS operations are typically designed for expected value of performance whereas inefficiency is caused by a variation in this value.

This paper is organized as follows. Section II introduces the concept of risk in TFM and describes methods to manage risk using stochastic programming. Section III describes the formulation of a stochastic TFM in the LP

framework. Section IV contains details of the Use Case which serves as the feasibility demonstration of the risk-management algorithm. Conclusions, summary, results, and directions for future work are presented in Section V.

II. The Concept of Risk in TFM and Risk-Management Using Stochastic Programming

Since risk is a concept that is used extensively in this work, it requires a definition at the outset. Every TFM algorithm based on optimization, for example, those listed in Section I, requires the minimization or maximization of a cost function. For instance, the BSP [23], BLO [41], and AAEP [42] models typically minimize the ground and airborne delays, number of cancelled flights, and the amount of deviation along a flight segment; or a combination of any of the above. Depending on the specific nature of the problem, additional components can also be introduced in the cost function. The TFM algorithm produces a set of directives, e.g. the amount of ground delay/stop or airborne holding and route selection. The optimization is subject to constraints on the dynamics of the flight and the available resources such as Sector capacity.

In the presence of capacity uncertainty, the cost function can take different values in response to a specific realization of the capacity constraint. For instance, if there is a probability associated with a downstream Sector for a flight being blocked, the flight may require a longer reroute. This paper defines Risk as the variation in the cost function in response to stochasticity. It needs to be clarified at the outset that Risk in the context of this work is not the probability that a flight will encounter weather. The TFM problem in this work requires all flights to avoid all given realizations of the weather.

A. Using the Spread of a Distribution to Characterize Risk

To further develop the concept of risk, Figure 6 presents a depiction of two probability distributions, both of which assign a probability to the value of an objective function. The first distribution has a considerably smaller "spread", and if the normal distribution is assumed, this translates into a smaller value of the variance. The implication of the smaller variance is that one can assure with 99.7% confidence that the value of the objective function, i.e. system delay, will be within the 3-sigma range of the expected delay. On the contrary, from the distribution on the right, the 99.7% confidence only exists for a significantly larger range around the expected value. A larger range of uncertainty has implications on efficient operation of airlines, especially in a hub-and-spoke configuration. If an airline is unable to guarantee with a high level of confidence that a flight will reach its destination within a certain range of its expected arrival time, then this may impact connecting flights and turn-around times significantly. Furthermore, the likelihood of an extreme event occurring, e.g. an extremely large deviation from the mean delay, is significantly higher when the spread of the distribution is large.

B. Relationship between Stochastic Weather and Capacity Uncertainty

Adverse weather directly affects NAS performance by limiting resources that may be available to the flights. As noted before, fog at the San Francisco International Airport often limits runway operations and impacts the aircraft acceptance or departure rates. In this work, the focus is on enroute capacity uncertainty, although the algorithms and analysis can be generalized to include airport capacity uncertainty.

Although Sector capacity determination is an open area of research [44-49], a starting point for nominal Sector capacity assessment is the Sector's Monitor Alert Parameter (MAP) value. The uncertainty in Sector capacity is most easily derived by an area-based measure, which calculates the area of overlap between the weather phenomenon in a realization, with the Sectors of interest. This is schematically shown in Figure 7, where a weather-affected area, depicted by the polygon, interacts with a Sector of interest, shaded in gray. Depending on what fraction of the Sector intersects with the weather, and given the probability of occurrence of a scenario, a histogram of capacities, ranging from zero to maximum capacity c_{max}, can be constructed. This procedure is independent of the LP formulation or solution and can be performed offline.

The quality of the histogram depends on the number of scenarios available, but only to an extent, since only integers can be used to represent MAP values.

C. Strategies for Risk Management

Several strategies may be employed to manage risk in TFM; some of which are described here. These are depicted in Figure 8. One possible strategy is to design a route that avoids the mean of all realizations of the weather. However, since there is a finite probability for each realization occurring (possibly based on forecast or simulations), the "mean weather" may never be realized, and a reroute will be required when one of the weather realization occurs. This is shown in Figure 8(a), where the planned route is shown as the dashed line. Consequently, a reroute will be required, depicted by the solid line. However, solving for a reroute once the flight has already departed on its nominal trajectory will require another TFM optimization problem, and the feasibility of the solution, i.e. a new feasible trajectory may not be available.

The second strategy, shown in Figure 8(b), is to calculate a reroute for all weather realizations, and travel on the mean path, depicted by the dashed line. However, this strategy does not mitigate the probability with which adverse weather will be encountered, and the flight will be forced to fall back on Strategy 1, i.e. plan a reroute from the point at which weather impacts the trajectory.

The third strategy, shown in Figure 8(c), is to travel on a route that avoids all simulated weather realizations. This is known as a risk-averse strategy, and can cause unnecessary delays especially if the weather realization did not ultimately require a longer reroute. Furthermore, there are no guarantees on the expected delay, although the variation in the delay may be small.

The fourth strategy, shown in Figure 8(d), divides the trajectory of an aircraft into two segments. The first segment is known as the first stage, and is common to all routes designed to avoid the weather realization. This is shown as the dark line in the figure. The second segment, known as the second stage or recourse stage, consists of reroutes designed to avoid each weather scenario provided to the flight, which are depicted by the lighter solid line, dashed line, and dotted line. The first stage trajectory is designed to guarantee feasibility of each of the recourse trajectories. Consequently, the flight does not need to solve another TFM problem if adverse weather is encountered. The strategy for a flight, i.e. the choice of a reroute in response to a weather realization, will affect the expected value of the system delay as well as its variation. When the TFM problem is solved by minimizing the expected

value of system delay over all scenarios, this is known as a risk-neutral strategy, and is generally posed as a two-stage stochastic linear program. This is described in the next section.

D. Stochastic Linear Program to Solve the Two-Stage Recourse Problem

Stochastic Linear Programs [50] (SLP) are generally modeled as two-stage recourse problems. The uncertainty in the problem is modeled by defining a finite number of scenarios $\{\omega_1, \omega_2, \dots \omega_k\}$ with associated probabilities of occurrence $\{p_1, p_2, \dots, p_k\}$. In the context of weather-related uncertainty, the values of $p_{1,\dots,k}$ can be obtained from probabilistic weather forecast, described in Section IIB.

The general form of a two-stage recourse problem is as follows

$$\max c^T x + \sum_{i=1}^{k} p_i r_i(x) \tag{1}$$

$$\text{subject to } \begin{matrix} Ax \le b \\ x \ge 0 \end{matrix}$$

$$\text{where } r_i(x) = \max g_i^T y_i \tag{2}$$

$$\text{subject to } \begin{matrix} T_i x + W_i y_i \le h_i \\ y_i \ge 0 \end{matrix}$$

In the foregoing equations, x is the first-stage decision variable that does not respond to the uncertain scenario ω. It is determined before any information regarding the uncertainty data has been obtained. On the other hand, y_i is the second-stage decision variable that is determined after deriving the observations regarding the uncertainties. Note that a different recourse decision y_i will be made when the ith scenario is realized. The goal of the two-stage model is to identify a first-stage solution x that is well-positioned against all possible manifestations of the uncertain scenarios in the future. An optimal first-stage solution x will tend to have the property that leaves the second stage in a position to exploit the advantageous scenarios without excessive vulnerability to disadvantageous scenarios.

The constraint matrix A and the constraint vector b are the deterministic constraints that are completely independent of the uncertainty. The objective function coefficients or cost for the first stage variables are given by c. The recourse costs $r_i(x)$ are a function of the first-stage decision x and the uncertain data associated with the ith scenario. The objective function coefficients or costs for the recourse variables are given by g_i. The uncertain constraints are defined by the matrices T_i and W_i and vector h_i, known as the technology matrix, recourse matrix, and resource vector, respectively. The two-stage recourse problem takes the following form:

$$\max \begin{bmatrix} c^\top & p_1 g_1^\top & p_2 g_2^\top & \cdots & p_k g_k^\top \end{bmatrix} \begin{bmatrix} x \\ y_1 \\ y_2 \\ \vdots \\ y_k \end{bmatrix}$$

$$\text{subject to } \begin{bmatrix} A & & & & \\ T_1 & W_1 & & & \\ T_2 & & W_2 & & \\ \vdots & & & \ddots & \\ T_n & & & & W_k \end{bmatrix} \begin{bmatrix} x \\ y_1 \\ y_2 \\ \vdots \\ y_k \end{bmatrix} \le \begin{bmatrix} b \\ h_1 \\ h_2 \\ \vdots \\ h_k \end{bmatrix} \tag{3}$$

$$x, y_1, y_2, \dots, y_k \ge 0$$

E. Exploring the Pareto Frontier in the Mean-Variance Tradeoff Space

The solution to the linear program given by Eq. (3) seeks to maximize the expected value (mean) of the cost over all possible scenarios. However this linear program does not explicitly consider the variance of the recourse costs over all possible scenarios. Modern Portfolio Theory (MPT) [34] states that the variance can be treated as a measure of risk and that there exists a trade-off in the mean-variance space as shown in Figure 9. Since the linear program given by Eq. (3) maximizes mean without considering the variance it gives the risk-neutral solution shown in Figure 9.

If the objective function seeks to minimize the variance of the recourse costs, the solution obtained will be the risk-averse solution. However, including the variance in the objective function will make the programming problem quadratic. The present research develops a linear programming formulation that generates the Pareto front of optimal solutions in the mean-variance space. Once the Pareto front is generated, the solution that maximizes the mean at a given level of acceptable risk can be determined as shown in Figure 9.

F. Generating the Pareto Frontier by Solving the LP with Reduced Variance

The problem of minimizing the variance in the recourse costs $r_1, r_2, \ldots, r_k$ for various scenarios $i = 1 \ldots k$ can be posed as a linear program similar to Eq. (3) with additional constraints that limit the deviation of the recourse cost from the mean recourse cost.

The first step is to solve the risk-neutral stochastic linear program given by Eq. (3). Let $\bar{r}$ denote the mean of the recourse costs over all possible scenarios for the solution to Eq. (3). The mean recourse cost can be calculated from the scenario costs as shown below:

$$\bar{r} = \sum_{i=1}^{k} p_i r_i \tag{4}$$

The deviation d_i of the recourse cost for the ith scenario from the mean recourse cost is given by the following expression:

$$d_i = r_i - \bar{r} \tag{5}$$

Let $D = \max_i |d_i|$ denote the maximum deviation over all scenarios. The main idea is to iteratively solve the linear program posed by Eq. (3), by adding constraints which limit the deviation of the recourse costs from the mean to be smaller than the maximum deviation at the previous iteration. Thus the additional constraint to be imposed for the ith scenario is given by the following:

$$|r_i - \bar{r}| \leq \alpha D, \;\; 0 < \alpha < 1 \tag{6}$$

The set of absolute value constraint shown in the foregoing equation can be replaced by the following two sets of linear constraints:

$$\begin{aligned} r_i - \bar{r} &\leq \alpha D \\ \bar{r} - r_i &\leq \alpha D \end{aligned} \tag{7}$$

This approach requires $2k$ additional constraints in the stochastic linear program. Since the recourse costs and their mean are linear functions of the decision variables, the constraints can be written as follows:

$$\begin{aligned} g_i^\top y_i - (p_1 g_1^\top y_1 \ + \cdots + p_i g_i^\top y_i + \cdots + p_k g_k^\top y_k) \le \alpha D \\ -g_i^\top y_i + (p_1 g_1^\top y_1 \ + \cdots + p_i g_i^\top y_i + \cdots + p_k g_k^\top y_k) \le \alpha D \end{aligned} \tag{8}$$

The modified linear program obtained upon inclusion of the $2k$ additional constraints is given as follows:

$$\max[\, c^\top \quad p_1 g_1^\top \quad p_2 g_2^\top \quad \ldots \quad p_k g_k^\top] \begin{bmatrix} x \\ y_1 \\ y_2 \\ \vdots \\ y_k \end{bmatrix}$$

$$\begin{bmatrix} A & & & & \\ T_1 & W_1 & & & \\ T_2 & & W_2 & & \\ \vdots & & & \ddots & \\ T_k & & & & W_k \\ & (1-p_1)g_1^\top & -p_2 g_2^\top & \cdots & -p_k g_k^\top \\ & (p_1-1)g_1^\top & p_2 g_2^\top & \cdots & p_k g_k^\top \\ & -p_1 g_1^\top & (1-p_2)g_2^\top & \cdots & -p_k g_k^\top \\ & p_1 g_1^\top & (p_2-1)g_2^\top & \cdots & p_k g_k^\top \\ & -p_1 g_1^\top & -p_2 g_2^\top & \cdots & (1-p_k)g_k^\top \\ & p_1 g_1^\top & p_2 g_2^\top & \cdots & (p_k-1)g_k^\top \end{bmatrix} \begin{bmatrix} x \\ y_1 \\ y_2 \\ \vdots \\ y_k \end{bmatrix} \le \begin{bmatrix} b \\ h_1 \\ h_2 \\ \vdots \\ h_k \\ \alpha D \\ \alpha D \\ \alpha D \\ \alpha D \\ \vdots \\ \alpha D \\ \alpha D \end{bmatrix} \tag{9}$$

$$x, y_1, y_2, \ldots, y_k \ge 0$$

It is worth noting that Eq. (8) can be modified so that the Pareto frontier exhibits different outcomes. For example, it may be of interest to penalize positive delays only, i.e. early arrivals are not penalized. In this case, only the first of the two constraints in Eq. (8) are necessary.

The next section formulates the risk-hedging stochastic LP for TFM.

III. Deterministic and Stochastic LP Formulation for TFM

A complete description of the Mixed-Integer Linear Program (MILP) formulation for Stochastic Air Traffic Flow Management Rerouting Problem (SATFMRP) is given in [41] and [42]. In this section, some of the key definitions and constraints are presented. The notation in this paper follows that used in [41] and [42], and the decision variable of interest will be referred to as the BLO variable.

A. Decision Variable and Data Sets

The variable of interest in this formulation is $x_{f,XY}^t$, a binary variable, i.e. 0 or 1. A value of 1 indicates that flight f (member of set $\mathcal{F}$), reaches Node Y from Node X, by time interval $t \in \mathcal{T}$ using an arc connecting the two nodes. Nodes X and Y belong to set $\mathcal{N}_f$ that is composed of all nodes on the route(s) of flight f. The sets $\mathcal{K}^d$ and $\mathcal{K}^a$ denote the set of nodes corresponding to departure and arrival airports, respectively. Since an airport in general is both a departure as well as an arrival airport, $\mathcal{K}^d \cap \mathcal{K}^a \neq \emptyset$. Let $k_f^d \in \mathcal{K}^d$ and $k_f^a \in \mathcal{K}^a$ denote departure and

arrival airport nodes for flight f, respectively. Node $q(k_f^d)$ denotes the departure airport boundary, and $p(k_f^a)$ denotes the arrival airport boundary. The distinction between an airport node and its boundary node is to allow for a detailed model for ground holds and runway delays.

The arc XY is a member of set $\mathcal{A}_f = \{XY | X, Y \in \mathcal{N}_f\}$ that is composed of all arcs on the route(s) of flight f. The set $\Gamma_f^+(X) = \{Y | XY \in A_f\}$ and $\Gamma_f^-(X) = \{Y | YX \in A_f\}$ are the set of nodes that have arcs from Node X and leading into Node Y respectively, for flight f.

Whereas sets $\mathcal{N}_f$ and $\mathcal{A}_f$ denote all possible nodes and all possible arcs for flight f, the sets $\mathcal{N}_f^* \subset \mathcal{N}_f$ and $\mathcal{A}_f^* \subset \mathcal{A}_f$ denote the nodes and arcs corresponding to the scheduled route of flight f. The variables $l_{f,XY}$, r_f, and d_f denote the travel time (number of time periods) for flight f over arc XY, the scheduled departure time period, and the scheduled arrival time period, respectively. It is noted in [42] that $l_{f,k_f^d,q(k_f^d)} = l_{f,p(k_f^a),k_f^a} = 0, \forall k_f^d \in \mathcal{K}^d, k_f^a \in \mathcal{K}^a$. In other words, a flight reaches the departure airport boundary immediately after leaving the departure airport node, and a flight reaches the arrival airport node immediately after leaving the arrival airport boundary. It also follows that

$$r_f = d_f + \sum_{XY \in A_f^*} l_{f,XY} \tag{10}$$

In other words, the scheduled arrival time of the flight is given by the sum of the departure time and flight times along scheduled route segments. Furthermore, $\bar{l}_{f,XY}$ and $\underline{l}_{f,XY}$ denote the maximum and minimum number of time segments for flight f on arc XY.

The 0-1 BLO variables can be used to determine quantities of interest for TFM. For instance, the time segment in which the flight f reaches node n is denoted by $T_{f,n}$ and given by the following summation:

$$T_{f,n} = \sum_{X \in \Gamma_f^-(Y)} \sum_{t \in \mathcal{T}} t\left(x_{f,XY}^t - x_{f,XY}^{t-1}\right) \tag{11}$$

It follows from Eq. (11) that given the time of entry at a node and the time of entry at a preceding node, the number of time intervals required to travel on the arc connecting the nodes can be calculated. Additional quantities such as sector counts (given the arcs belonging to a sector) can also be calculated, as detailed in [41] and [42].

B. Constraint Formulation

The variables are linked with constraints resulting from the spatio-temporal definition of the graph. The so-called flight structure constraints define the continuity in time and space for a flight. The temporal continuity constraints [42] are represented by the following linear inequalities and equalities:

$$\begin{aligned} x_{f,XY}^{t-1} &\le x_{f,XY}^t, \qquad t \in \mathcal{T}_{f,XY}^*, (X,Y) \in \mathcal{A}_f, f \in \mathcal{F} \\ x_{f,XY}^{t-1} &= x_{f,XY}^t, \qquad t \in \mathcal{T}_{f,XY} \setminus \mathcal{T}_{Xf,Y}^*, (X,Y) \in \mathcal{A}_f, f \in \mathcal{F} \end{aligned} \tag{12}$$

where $\mathcal{T}_{f,XY}^*$ is the set of feasible time units in which a flight f can reach Node Y from Node X over the arc connecting the two nodes, and $\mathcal{T}_{f,XY}$ is the smallest set of consecutive time intervals that contains $\mathcal{T}_{f,XY}^*$. These

constraints state that if a flight was in node X by time period t, then this must also hold true for any later time period $t' > t$.

The spatial continuity constraints [42] are given by the following inequalities:

$$\sum_{Z \in \Gamma_f^+(Y)} x_{f,YZ}^{t+\underline{l}_{f,YZ}} \leq \sum_{X \in \Gamma_f^-(Y)} x_{f,XY}^{t} \leq \sum_{Z \in \Gamma_f^+(Y)} x_{f,YZ}^{t+\bar{l}_{f,YZ}}, \qquad t \in \mathcal{T}_{f,Y}, Y \in \mathcal{N}_f \backslash \{k_f^d, k_f^a\}, f \in \mathcal{F} \tag{13}$$

In the foregoing, $\mathcal{T}_{f,Y}$ denotes the set of all times units by which a flight f can reach Node Y from any other node along the route of that flight. Spatial continuity constraints force connectivity through a node.

The third set of constraints is composed of those that are derived from airspace capacity. To formulate the problem with capacity constraints, the sets $\mathcal{N}_f^{j+}$ and $\mathcal{N}_f^{j-}$ are defined for a flight f in the jth Sector, as the set of nodes entering and leaving the jth Sector. The sector capacity constraints are given by the following [42]:

$$\sum_{f \in \mathcal{F}} \left[\sum_{Y \in \mathcal{N}_f^{j+}} \sum_{X \in \Gamma_f^-(Y)} x_{f,XY}^{t} - \sum_{Y \in \mathcal{N}_f^{j-}} \sum_{X \in \Gamma_f^-(Y)} x_{f,XY}^{t} \right] \leq S_j^t, \qquad t \in \mathcal{T}, j \in \mathcal{J} \tag{14}$$

The term inside the first summation of Eq. (14) is equal to 1 only if a flight is in Sector j at time t, and equal to 0 if it has not yet entered or has already left Sector j at time t. When summed over all flights, this counts the total number of flights in Sector j at time t. This number is constrained to be less than the Sector capacity at that time, S_j^t, for a Sector $j \in \mathcal{J}$.

Capacity constraints can be derived for airport arrival and departure capacity, but were not used in this work. Mechanisms to include arrival and departure capacity constraints are described in [23], which can also explicitly model scenarios where the arrival and departure capacity are dependent on each other due to simultaneous operation on the same set of runways [51].

C. Cost Function Formulation

In the BLO model, the cost J has contributions from different components, depending on the modeling requirements of the problem. A comprehensive list is presented in [42], which not only includes the components presented in [41], but also introduces additional terms for greater flexibility in formulating TFM problems. In this work, the number of cancelled flights, overall flight ground delays, and airborne delays were penalized. These three cost function components, denoted by J_{cancel}, J_{ground}, and J_{airborne}, are listed as follows:

$$J_{\text{cancel}} = -\sum_{f \in \mathcal{F}} x_{f,k_f^d,q\left(k_f^d\right)}^{t}, \qquad t = \max \mathcal{T}_{f,k_f^d,q\left(k_f^d\right)} \tag{15}$$

$$J_{\text{ground}} = \sum_{f \in \mathcal{F}} \sum_{t \in \mathcal{T}_{f,k_f^d,q\left(k_f^d\right)}} c_{f,G}(t) \left(x_{f,k_f^d,q\left(k_f^d\right)}^{t} - x_{f,k_f^d,q\left(k_f^d\right)}^{t-1} \right) \tag{16}$$

$$J_{\text{airborne}} = \sum_{f\in\mathcal{F}}\left[\sum_{t\in\mathcal{T}_{f,p\left(k_f^a\right),k_f^a}} c_{f,T}(t)\left(x^{t}_{f,p\left(k_f^a\right),k_f^a} - x^{t-1}_{f,p\left(k_f^a\right),k_f^a}\right) - \sum_{t\in\mathcal{T}_{f,k_f^d,q\left(k_f^d\right)}} c_{f,G}(t)\left(x^{t}_{f,k_f^d,q\left(k_f^d\right)} - x^{t-1}_{f,k_f^d,q\left(k_f^d\right)}\right)\right] \tag{17}$$

where $c_{f,T}(t) = c_T \cdot \left(t - r_f\right)$ and $c_{f,G}(t) = c_G \cdot \left(t - d_f\right)$ (with constant c_T and c_G) are coefficients such that each additional unit of delay from scheduled arrival and departure has a proportionately heavier penalty.

D. Stochastic LP Formulation

The foregoing development has been used extensively for deterministic TFM. In the presence of stochastic capacity constraints, the Sector capacities S_j^t in Eq. (14) are uncertain quantities, and as described earlier can be sampled based on scenarios. The set of first stage variables for the TFM problem are then composed of all the decision variables that are unaffected by stochastic capacity. In the context of TFM, these variables correspond to the segment of a flight prior to any Sector whose capacity is stochastic. All variables that do not belong to the first stage then belong to the recourse stage. It is easy to see from Eq. (9) that the technology matrices T_i and recourse matrices W_i are respectively the same regardless of the scenario, and vectors h_i correspond to different scenarios of the capacity constraint given by Eq. (14).

IV. A Use Case in Stochastic Traffic Flow Management

The foregoing development of the SLP is now applied to a Use Case. Figure 10 shows the area of interest, viz. the north-eastern portion of the continental United States. Five Air Route Traffic Control Centers (ARTCC) are considered in the present Use Case: Boston (ZBW), Washington, D.C. (ZDC), Indianapolis (ZID), New York (ZNY), and Cleveland (ZOB). Five airports are included in the example: Logan International Airport (BOS), Ronald Reagan Washington National Airport (DCA), Detroit Metropolitan Wayne County Airport (DTW), LaGuardia Airport (LGA), and a pseudo-airport LVT. The pseudo-airport is a waypoint from the Coded Instrument Flight Procedures (CIFP) database that lies along or near routes for flights originating from Dallas-Fort Worth International Airport (DFW) and George Bush Intercontinental Airport (IAH) that were not included in the analysis because they lie outside the geographical area of interest. The airport DTW is also located close to the jet-routes for flights originating from the west coast.

The Centers are subdivided into Sectors. This is because stochastic capacity constraints are more readily enforced at the Sector level than at the Center level, due to the availability of MAP values as a notion of capacity. The choice of Sectors in the Use Case has been restricted to those that correspond to the cruise altitude of aircraft. This results in the airspace of interest being divided into 89 Sectors, including those from Atlanta ARTCC (ZTL). Enroute Sectors from ZTL are also included in this analysis because flights from LVT to DCA, LGA, or BOS may be redirected through ZTL in the presence of inclement weather. It should be noted that the number of Sectors used

in the LP formulation ultimately depends on the number of Sectors actually encountered by the modeled flights and their routes.

A. Use Case Formulation

Five weather scenarios are used to introduce stochastic Sector capacities. The weather scenarios were generated using echo tops from the NOAA website and superimposed upon the area of interest, as shown in Figure 11(a) through Figure 11(e). The shape, size, and location of the echo tops were randomly altered in each scenario to cover different parts of the Sector layout. Each echo top is converted into a set of distinct convex polygons using k-means clustering.

Nominal trajectories are first generated, in the absence of weather. These paths are used to solve the deterministic TFM problem with rerouting and serve as the benchmark against which delays in the system are evaluated. The nominal trajectories between all airport pairs are shown in Figure 12 as solid lines. These trajectories were generated using an A* search among the waypoints from the CIFP database, using distance from the destination as the criterion, and do not necessarily correspond to operationally viable routes. The relevant waypoints in the region of interest are also shown in this figure, as grey dots.

A composite of the five weather scenarios is depicted by the shaded area in Figure 12, which depicts the graph-based abstraction of the NAS It may be observed that all of the nominal trajectories intersect with Sectors that are affected by at least one weather scenario. The next step in the development of the Use Case is the identification of common paths for multiple routes for a given airport pair. Thereafter, reroutes for each weather realization are calculated from these points. The common segments correspond to the first stage of the stochastic program, and each of the reroutes starting from the end of the common segment corresponds to a set of recourse variables.

The stochastic LP is formulated for a 15 flight example, all of which depart their airports at time $t = 1$. The airport pairs are chosen arbitrarily and are given by: LVT-BOS, LVT-DTW, LVT-LGA, LVT-DCA, LGA-LVT, LGA-DTW, DCA-DTW, DTW-LGA, LGA-LVT, LVT-BOS, LVT-LGA, BOS-LVT, LGA-DTW, DTW-BOS, DTW-LGA. All routes between airport pairs are discretized into a network of nodes connected by arcs. The nodes are obtained by calculating the intersection of each route with the Sectors the flight passes through. This results in the set $\mathcal{A}_f$ of node pairs XY.

It is assumed that all flights are cruising with a true airspeed of 400kts. Based on the length of each segment, the amount of time is calculated, i.e. the constants $l_{f,XY}$ defined in Section IIIA. To reduce the complexity of the problem, all values are scaled by a discrete time step of 4 minutes and then rounded (floored) to the nearest integer.

The structure of the constraint matrix is shown in Figure 13. The LP is composed of 731 first stage variables and 4895 recourse variables per scenario; a total of 27208 variables (accounting for additional variables for segment-length and path-length deviations). A total of 99460 constraints are generated. The matrix is 99.97% sparse, with 337402 non-zero variables.

The matrix structure for the risk-neutral problem clearly exhibits the Benders' decomposition [52] blocks, with the first stage block (A matrix) in the top left corner, and the five T and W blocks along the rows and the diagonal. For the risk-hedged problem, additional constraints are introduced which link all the stages. Additionally, each block

exhibits the so-called Dantzig-Wolfe decomposition [53], with matrices along a row depicting the master problem, and fifteen blocks along the diagonal of a Bender's block depicting the subproblem for each aircraft. Note that the subproblem blocks are of different size because the number of variables required for each flight depends on the number of segments along the path.

B. Use Case Results

The nominal route solver, risk-neutral case, and risk-averse cases are solved independently. Since the flight time in a link is considered fixed, i.e. $l_{f,XY} = \bar{l}_{f,XY} = \underline{l}_{f,XY}$, path-stretching is not permitted as a solution to the LP, and no airborne delays are obtained. Instead, the solution attributes all delays to ground stops. An example of a ground stop due to downstream Sector capacity constraints is shown in Figure 14.

As mentioned before, all flights have a scheduled departure time of $t = 1$. In this example, two flights from LVT are shown in Figure 14, with Figure 14(a) depicting a flight to LGA, and Figure 14(b) depicting a flight to DCA. The scheduled departure and arrival times for the two flights result in a downstream Sector capacity constraint being violated. As a consequence, the flight to DCA is delayed by one time unit. This figure shows multiple trajectories; the choice of which depends on the actual scenario being realized.

Figure 15 shows the trajectories followed by a flight from LGA to DTW, with Figure 15(a) depicting the risk-neutral strategy and Figure 15(b) depicting the risk-averse strategy. In both figures, the solid lines depict the routes followed by a flight for all realizations of the weather, except for Scenario 3. If Scenario 3 occurs, the shaded area depicts the coverage of Sectors by inclement weather. In the risk-neutral strategy, the dashed line depicts the trajectory followed upon the realization of Scenario 3. Note that the entry and exit times over the common segment are identical. In the risk-averse case, it may be observed that flight follows the same trajectory, a route that avoids all weather-impacted areas in all scenarios. The risk-averse strategy results in the flight always requiring 22 units of time, whereas the risk-neutral trajectory can require 21 or 22 units of time, depending on which weather scenario is realized.

C. Analysis of the Risk-Hedging Strategy

Figure 16 shows the relative frequency histogram for flight delays, for a variety of risk-hedging strategies. The delays for a strategy are calculated by subtracting the nominal flight times (obtained by solving the LP for flights with no stochastic weather constraints) from the flight times obtained from a risk-hedging LP. Over a scenario, all deviations from scheduled are summed; the result is termed the 'system delay'. Note that the formulation used in this example penalizes all deviations from the scheduled time, including negative delays, i.e. arrivals before scheduled time. It is possible to penalize only positive delays, by removing the absolute sign in Eq. (6). In the Use Case, all delays are positive since the scheduled time of flight is equal to the time of flight along the nominal trajectory, and the time of flight on any other route other than the nominal route is larger than that for the nominal trajectory. The mean delay is calculated by adding the system delays weighted by the probability of the scenario.

In the top left, the histogram for the risk-neutral strategy is depicted. The solid line in all the figures is used to depict the expected value of the delay time. The expected value of delay as a result of the risk-neutral strategy is

approximately 4 time units. The presence of an outlier results in a Maximum Absolute Deviation (M.A.D.) of approximately 20 time units.

Next, a risk-hedging constraint is imposed such that the permitted M.A.D. is 0.67 times the risk-neutral M.A.D. The resulting histogram is shown on the top right of Figure 16. It is observed that the expected delay increases to approximately 10 time units, and the M.A.D. reduces to approximately 14 time units, which is approximately 67% of 20 time units.

The bottom left of Figure 16 corresponds to a permitted M.A.D. that is 0.13 times the risk-neutral M.A.D. This strategy results in an increase in the expected value of the delay to 24 units. However, the M.A.D. reduces to 3 time units, which is approximately 13% of 20 time units.

Finally, on the bottom right, the result for the risk-averse strategy is shown. This strategy results in all flights flying along the risk-averse route that circumvents all weather phenomena. The expected delay increases to 30 time units and there is no variation in the delay since all flights follow the risk-averse trajectory regardless of which of the five weather scenarios has been realized.

Although results corresponding to four values of the parameter α are shown in Figure 16, analysis on the Use Case was carried out by first starting with the risk-neutral value of M.A.D. and using the floor operator to set the value as risk-hedging constraint on the stochastic LP. At the end of an iteration, a new value of M.A.D. and expected delay were calculated. The parameter α is equal to the ratio of the new M.A.D. and the risk-neutral M.A.D. This process is iterated until the M.A.D. is equal to zero, or no feasible solution is obtained. The result of this iteration is shown in Figure 17. The solution for each iterated value of α is depicted by a circle, and is a Pareto-optimal solution because it is the solution with minimum cost which satisfies the maximum absolute deviation bound. The Pareto frontier is not necessarily convex because only integer solutions are allowed in the problem. The four strategies with different values of the iterating parameter α are also shown on this figure.

D. Computational Aspects of the Problem

It is clear from Section IVA that the stochastic TFM problem can result in very large scale LPs when considering a NAS-wide solution, or for a large number of flights. The Use Case described in the foregoing requires approximately 2 hours of computation using a simplex solver from the GNU Linear Programming Kit (GLPK) [54] on a single core of a 2.4GHz processor. When the problem is expanded to the NAS, the number of first stage variables is expected to increase significantly, but the number of recourse variables can remain bounded especially when weather realizations are confined to a smaller region of the airspace. For example, capacity uncertainty due to inclement weather on the East Coast will not likely affect flights whose operations are restricted to the West Coast. Moreover, the number of variables is dependent on the time interval used for discretizing the problem, and the total time horizon over which the solution is desired.

Computational efforts directed towards solving large-scale LPs is still an area of active research, and a full description is beyond the scope of this paper, which is concerned largely with developing a novel framework for risk-hedged TFM. However, there are several points that support the feasibility of applying the risk-hedged TFM algorithm described in this paper, to larger, NAS-level problems. For example, it should be noted that the GLPK implementation of the Use Case did not exploit any specific sparsity pattern or block decomposition. Decomposition

techniques for the TFM problem have been described in [55,56]. Recent results described in [57] show that a parallel implementation of Dantzig-Wolfe decomposition on Graphics Processing Units can solve very large problems with high computational efficiency in real time. Implementation of the risk-hedged TFM algorithm on these platforms is a subject of future research.

V. Conclusions

This paper demonstrated the feasibility of a new approach to actively manage the risk induced in traffic flow management due to the stochasticity of adverse weather. A novel approach has been developed that achieves the following: 1) a preliminary definition of risk in traffic flow management due to weather stochasticity and demonstrated the applicability of performance-risk tradeoff concepts from Modern Portfolio Theory; 2) an approach to map the impact of stochastic adverse weather in terms of the National Airspace System capacity uncertainty; 3) risk-management strategies in the Linear Programming framework, and 4) the active control of variance in system performance, by sacrificing the expected value of cost. This guarantees the performance bounds on the traffic flow management algorithm, while also assuring robustness in the solution.

A Use Case scenario was presented that reflects National Airspace System operations on a regional scale. The Use Case work flow can be extended to more complex networks such as a system-wide formulation for the entire National Airspace with several thousand flights. The work advanced in this paper can form the basis for the development of a decision support tool. Additional extensions include mechanisms for incorporating user preferences in stochastic traffic flow management. Moreover, substantial improvements in the solution speed are feasible through the use high-performance computing hardware. For instance, the Linear Program is amenable to decomposition techniques and parallel implementation on Graphics Processing Units. These platforms offer considerable advantages over standard Linear Program solvers in that they can be used to solve several large scale problems with a large number of scenarios and flights in an efficient manner and in real time.

Acknowledgments

This research was supported by NASA Contract No. NNX12CD12P, with Dr. Deepak Kulkarni of NASA Ames Research Center serving as the Technical Monitor. The authors thank Dr. Sai Vaddi for his valuable suggestions for improving the optimization algorithm.

References

[1] Wearden, G.. “Ash cloud costing airlines £130m a day,” The Guardian (London), retrieved April 17, 2010.

[2] “Flight disruptions cost airlines $1.7bn, says IATA,” BBC News, April 21, 2010. Retrieved April 24, 2011.

[3] Stefanidis, K., Klimenko, V., Krozel, J., “Impact Analysis for Volcanic Ash Hazards,” *AIAA Guidance Navigation and Control Conference*, Portland, OR, Paper AIAA 2011-6692, Aug. 2011. doi: 10.2514/6.2011-6692

[4] Rose, W. I., “Interaction of Aircraft and Explosive Eruption Clouds - A Volcanologist's Perspective,” *AIAA Journal*, Vol. 25, No. 1, Jan. 1987, pp. 25-28.

doi: 10.2514/3.9579

[5] Kim, J., Palaniappan, K., Menon, P. K., Nag, M., and Subbarao, K., "Trajectory Uncertainty Modeling for Queuing Analysis of the National Airspace System," *The 26th Congress of ICAS and 8th AIAA Aviation Technology, Integration, and Operations Conference*, Anchorage, AK, Paper AIAA 2008-8554, Sep. 2008.
doi: 10.2514/6.2008-8854

[6] Kim, J., Tandale, M. D., and Menon, P. K., "Air-Traffic Uncertainty Models for Queuing Analysis," *9th AIAA Aviation Technology, Integration, and Operations Conference*, Hilton Head, SC, Paper AIAA 2009-7053, Sep. 2009.
doi: 10.2514/6.2009-7053

[7] Krozel, J., "Survey of Weather Impact Models Used in Air Traffic Management," *10th AIAA Aviation Technology, Integration, and Operations Conference*, Fort Worth, TX, Paper AIAA 2010-9020, Sep. 2009.
doi: 10.2514/6.2010-9020

[8] Grabbe, S., Sridhar, B., and Mukherjee, A., "Central East Pacific Flight Scheduling," *AIAA Guidance, Navigation, and Control Conference and Exhibit*, Hilton Head, SC, Paper AIAA 2007-6447, Aug. 2007.
doi: 10.2514/6.2007-6447

[9] Andreatta, G. and Romanin-Jacur, G., "Aircraft Flow Management Under Congestion," *Transportation Science*, Vol. 21, No. 4, Nov. 1987, pp. 249-253.
doi: 10.1287/trsc.21.4.249

[10] Terrab, M. and Odoni, A. R., "Strategic Flow Management for Air Traffic Control," *Operations Research*, Vol. 41, No. 1, Jan.-Feb. 1993, pp. 138-152.
doi: 10.1287/opre.41.1.138

[11] Richetta, O. and Odoni, A. R., "Solving Optimally the Static Ground-Holding Policy Problem in Air Traffic Control," *Operations Research Society of America*, Vol. 27, No. 3, Aug. 1993, pp. 228-238.
doi: 10.1287/trsc.27.3.228

[12] Richetta, O. and Odoni, A. R., "Dynamic Solution to the Ground-Holding Problem in Air Traffic Control," *Transportation Research Part A: Policy and Practice*, Vol. 28, No. 3, May 1994, pp. 167-185.
doi: 10.1016/0965-8564(94)90015-9

[13] Rikfin, R. M., *The Single Airport Static Stochastic Ground Holding Problem*, Master's Thesis, Massachusetts Institute of Technology, 1994.

[14] Hoffman, R. L., *Integer Programming Models for Ground-Holding in Air Traffic Flow Management*, Ph.D. Dissertation, University of Maryland at College Park, 1997.

[15] Mukherjee, A. and Hansen, M., "A Dynamic Stochastic Model for the Single Airport Ground Holding Problem," *Transportation Science*, Vol. 41, No. 4, Nov. 2007, pp. 444-456.
doi: 10.1287/trsc.1070.0210

[16] Liu, P.-C. B., Hansen, M., and Mukherjee, A., "Scenario-Based Air Traffic Flow Management: From Theory to Practice," *Transportation Research Part B: Methodological*, Vol. 42, Nos. 7-8, Aug. 2008, pp. 685-702.
doi: 10.1016/j.trb.2008.01.002

[17] Vranas, P. B., Bertsimas, D. J., and Odoni, A. R., "Dynamic Ground-Holding Policies for a Network of Airports," *Transportation Science*, Vol. 28, No. 4, Nov. 1994, pp. 275-291.
doi: 10.1287/trsc.28.4.275

[18] Vranas, P. B., Bertsimas, D. J., and Odoni, A. R., "The Multi-Airport Ground-Holding Problem in Air Traffic Control," *Operations Research*, Vol. 42, No. 2, Mar.-Apr 1994, pp. 249-261.
doi: 10.1287/opre.42.2.249

[19] Navazio, L. and Romanin-Jacur, G., "The Multiple Connections Multi-Airport Ground-Holding Problem: Models and Algorithms," *Transportation Science*, Vol. 32, No. 3, Aug. 1998, pp. 268-276.
doi: 10.1287/trsc.32.3.268

[20] Helme, M. P., "Reducing Air Traffic Delay in a Space-Time Network," *Proceedings of the IEEE International Conference on Systems, Man, and Cybernetics*, Chicago, IL, Vol. 1, Oct. 1992, pp. 236-242.
doi: 10.1109/ICSMC.1992.271770

[21] Mukherjee, A. and Hansen, M., "A Dynamic Rerouting Model for Air Traffic Flow Management," *Transportation Research Part B: Methodological*, Vol. 43, No. 1, Jan. 2009, pp. 159-171.
doi: 10.1016/j.trb.2008.05.011

[22] Rios, J., and Morando. A., "The Value of Reduced Uncertainty in Air Traffic Flow Management," *AIAA Guidance Navigation and Control Conference*, Portland, OR, Paper AIAA 2011-6512, Aug. 2011.
doi: 10.2514/6.2011-6512

[23] Bertsimas, D. and Patterson, S. S., "The Air Traffic Flow Management Problem with Enroute Capacities," *Operations Research*, Vol. 46, No. 3, May-Jun. 1998, pp. 406-422.
doi: 10.1287/opre.46.3.406

[24] Bertsimas, D. and Patterson, S. S., "The Traffic Flow Management Rerouting Problem in Air Traffic Control: A Dynamic Network Flow Approach," *Transportation Science*, Vol. 34, No. 3, Aug. 2000, pp. 239-255.
doi: 10.1287/trsc.34.3.239.12300

[25] Sridhar, B., Grabbe, S., and Mukherjee, A., "Modeling and Optimization in Traffic Flow Management," *Proceedings of the IEEE*, Vol. 96, No. 12, Dec. 2008, pp. 2060-2080.
doi: 10.1109/JPROC.2008.2006141

[26] Meyn, L., "Probabilistic Methods for Air Traffic Demand Forecasting," *AIAA Guidance, Navigation, and Control Conference*, Monterey, CA, Paper AIAA 2002-4766, Aug. 2002.
doi: 10.2514/6.2002-4766

[27] Gilbo, E. P. and Smith, S. B., "A New Model to Improve Aggregate Air Traffic Demand Predictions," *AIAA Guidance, Navigation, and Control Conference*, Paper AIAA-2007-6450, Hilton Head, SC, Aug. 2007.
doi: 10.2514/6.2007-6450

[28] Gilbo, E. P. and Smith, S. B., "Probabilistic Predictions of Traffic Demand for En Route Sectors Based on Individual Flight Data," Tech. Rep. VNTSC-TFM-10-01, Volpe National Transportation Systems Center, Jan. 2010.

[29] Chatterji, G., Sridhar, B., Sheth, K., Kim, D., and Mulfinger, D., "Methods for Establishing Confidence Bounds on Sector Demand Forecasts," *AIAA Guidance, Navigation, and Control Conference*, Providence, RI, Paper AIAA 2004-5232, Aug. 2004.
doi: 10.2514/6.2004-5232

[30] Wanke, C. R., Callaham, M. B., Greenbaum, D. P., and Masalonis, A. J., "Measuring Uncertainty in Airspace Demand Predictions for Traffic Flow Management Applications," *AIAA Guidance, Navigation, and Control Conference*, Austin, TX, Paper AIAA 2003-5708, Aug. 2003.
doi: 10.2514/6.2003-5708

[31] Chen, N. and Sridhar, B., "Management-Action-Embedded Sector-Demand Prediction Models," *Journal of Guidance, Control, and Dynamics*, Vol. 33, No. 6, Nov.-Dec. 2010, pp. 1892–1898.
doi: 10.2514/1.46903

[32] Wanke, C. R., Mulgund, S., Greenbaum, D. P., and Song, L., "Modeling Traffic Prediction Uncertainty for Traffic Management Decision Support," *AIAA Guidance, Navigation, and Control Conference*, Providence, RI, Paper AIAA 2004-5230, Aug. 2004.
doi: 10.2514/6.2004-5230

[33] Krozel, J., Rosman, D., and Grabbe, S., "Analysis of En Route Sector Demand Error Sources," *AIAA Guidance, Navigation, and Control Conference*, Monterey, CA, Paper AIAA 2002-5016, Aug. 2002.
doi: 10.2514/6.2002-5016

[34] Benninga, S., *Financial Modeling*, MIT Press, Cambridge, MA, 2008.

[35] Agustin, A., Alonso-Ayuso, A., Escudero, L. F., and Pizarro, C., "On Air Traffic Flow Management with Rerouting. Part II: Stochastic Case," *European Journal of Operational Research*, Vol. 219, No. 1, May 2012, pp. 167-177.
doi: 10.1016/j.ejor.2011.12.032

[36] Hoffman, B., Krozel, J., Davidson, G., and Kierstead, D. "Probabilistic Scenario-Based Event Planning for Traffic Flow Management," *AIAA Guidance, Navigation, and Control Conference and Exhibit*, Hilton Head, SC, Paper AIAA 2007-6361, Aug. 2007.
doi: 10.2514/6.2007-6361

[37] Alonso, A., Escudero, L. F., and Ortuno, M. T., "A Stochastic 0-1 Program Based Approach for the Air Traffic Flow Management Problem," *European Journal of Operational Research*, Vol. 120, No. 1, Jan. 2000, pp. 47-62.
doi: 10.1016/S0377-2217(98)00381-6

[38] Chang, Y., *Stochastic Programming Approaches to Air Traffic Flow Management Under the Uncertainty of Weather*, Ph.D. Dissertation, Georgia Institute of Technology, December 2010.

[39] Agustin, A., Alonso-Ayuso, A., Escudero L. F., and Pizarro C., "Mathematical Optimization Models for Air Traffic Flow Management: A Review," *Improving Risk Management*, Technical Report 2010.06, Universidad Rey Juan Carlos, 2010.

[40] Clare, G., and Richards, A., "Air Traffic Flow Management Under Uncertainty: Application of Chance Constraints," *Proceedings of the 2nd International Conference on Application and Theory of Automation in Command and Control Systems*, London, UK, May 2012, pp. 20-26.

[41] Bertsimas, D., Lulli, G., and Odoni, A., "An Integer Optimization Approach to Large-Scale Air Traffic Flow Management," *Operations Research*, Vol. 59, No. 1, Jan.-Feb. 2011, pp. 211-227.
doi: 10.1287/opre.1100.0899

[42] Agustin, A., Alonso-Ayuso, A., Escudero, L. F., and Pizarro, C., "On Air Traffic Flow Management with Rerouting. Part I: Deterministic Case," *European Journal of Operational Research*, Vol. 219, No. 1, May 2012, pp. 156-166.
doi: 10.1016/j.ejor.2011.12.021

[43] Mitchell, J. S. B., Polishchuk, V., and Krozel, J., "Airspace Throughput Analysis Considering Stochastic Weather," *AIAA Guidance, Navigation, and Control Conference*, Keystone, CO, Paper AIAA 2006-6770, Aug. 2006.
doi: 10.2514/6.2006-6770

[44] Krozel, J., Mitchell, J. S. B., Polishchuk, V., and Prete, J., "Capacity Estimation for Airspaces with Convective Weather Constraints," *AIAA Guidance, Navigation, and Control Conference*, Hilton Head, SC, Paper AIAA 2007-6451, Aug. 2007.
doi: 10.2514/6.2007-6451

[45] Zou, J., Krozel, J. W., and Mitchell, J. S. B., "Two Methods for Computing Directional Capacity given Convective Weather Constraints," *AIAA Guidance, Navigation, and Control Conference*, Chicago, IL, Paper AIAA 2009-6197, Aug. 2009.
doi: 10.2514/6.2009-6197

[46] Klein, A., Cook, L., and Wood, B., "Airspace Availability Estimation for Traffic Flow Management Using the Scanning Method," *Digital Avionics Systems Conference*, St. Paul, MN, Oct. 2008, pp. 3.B.5–1 – 3.B.5–10.
doi: 10.1109/DASC.2008.4702802

[47] Welch, J. D., Andrews, J. W., Martin, B. D., and Sridhar, B., "Macroscopic Workload Model for Estimating En Route Sector Capacity," *7th ATM Seminar*, Barcelona, Spain, Paper 37, Jul. 2007.

[48] Majumdar, A., Ochieng, W. Y., McAuley, G., Lenzi, J. M., and Lepadatu, C., "The Use of Panel Data Analysis Techniques in Airspace Capacity Estimation," *Air Traffic Control Quarterly*, Vol. 14, No. 1, 2006, pp. 95–115.

[49] Welch, J. D., Andrews, J. W., Martin, B. D., and Shank, E. M., "Applications of a Macroscopic Model for En Route Sector Capacity," *AIAA Guidance, Navigation, and Control Conference*, Honolulu, Hawaii, Paper AIAA 2008-7221, Aug. 2008.
doi: 10.2514/6.2008-7221

[50] Kall, P., and Mayer, J., *Stochastic Linear Programming*, Kluwer Academic Press, New York, NY, 2005.

[51] Airport Capacity Benchmark Report 2004, prepared by the MITRE Corporation for FAA, September 2004. Available at http://www.faa.gov. Retrieved February 11, 2014.

[52] Benders, J. F., "Partitioning Procedures for Solving Mixed-Variables Programming Problems," *Numerische Mathematik*, Vol. 4, No. 1, Dec. 1962, pp. 238-252.
doi: 10.1007/BF01386316

[53] Dantzig G B., and Wolfe P., "Decomposition Principle for Linear Programs," *Operations Research*, Vol. 8, No. 1, Jan.-Feb. 1960, pp. 101-111.
doi: 10.1287/opre.8.1.101

[54] GNU Linear Programming Kit, http://www.gnu.org/software/glpk/glpk.html

[55] Rios, J., and Ross, K., "Massively Parallel Dantzig-Wolfe Decomposition Applied to Traffic Flow Scheduling," *Journal of Aerospace Computing, Information, and Communication*, Vol. 7, No. 1, Jan. 2010, pp. 32-45.
doi: 10.2514/1.45606

[56] Wei, P., Cao, Y., and Sun, D., "Total Unimodularity and Decomposition Method for Large-Scale Air Traffic Cell Transmission Model," *Transportation Research Part B: Methodological*, Vol. 53, Jul. 2013, pp. 1-16.
doi: 10.1016/j.trb.2013.03.004

[57] Tandale, M. D., Wiraatmadja, S., Vaddi, V. V., and Rios, J. L., "Massively Parallel Optimal Solutions to the Nationwide Traffic Flow Management Problem," *AIAA Aviation Technology, Integration, and Operations Conference*, Los Angeles, CA, Paper AIAA 2013-4349, Aug. 2013.
doi: 10.2514/6.2013-4349

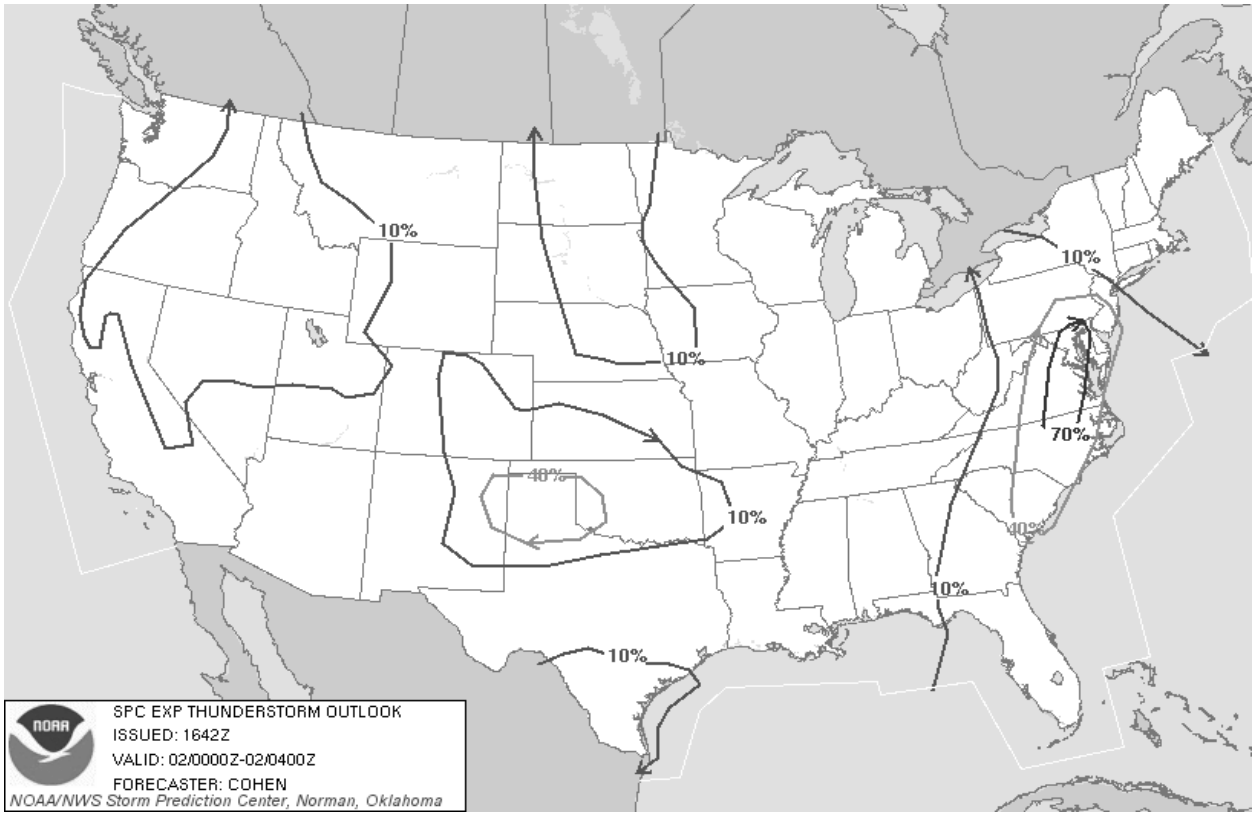

Figure 1. NOAA Experimental Thunderstorm Outlook Probability Curves of Weather Impact (http://www.spc.noaa.gov/products/exper/enhtstm/)

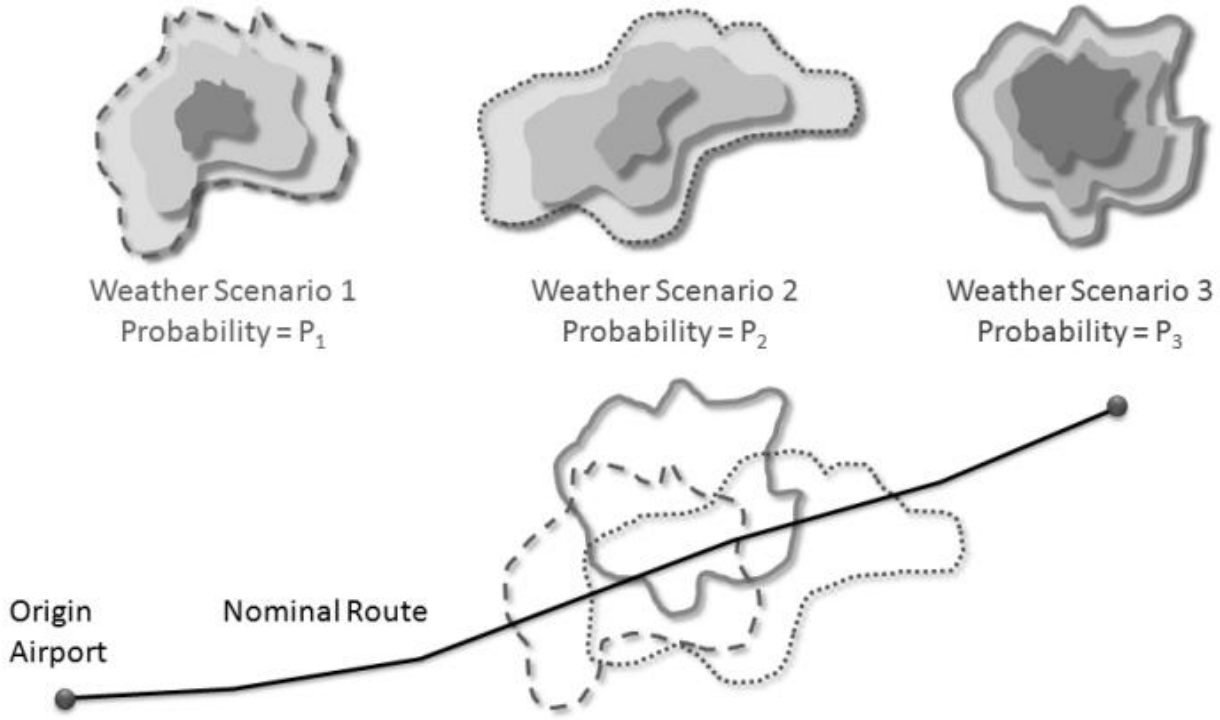

Figure 2. Weather Scenarios and Flight Routes in Response to Scenario Realization

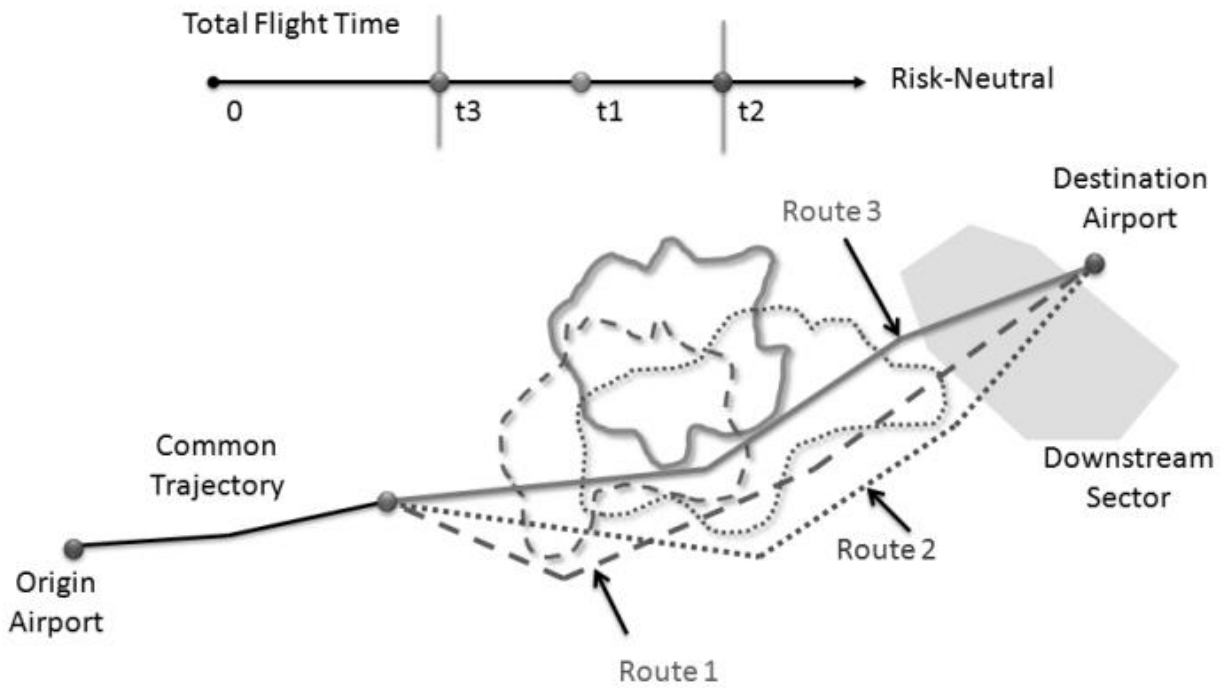

Figure 3. Risk Neutral Strategy for Rerouting in Response to Weather Hazard

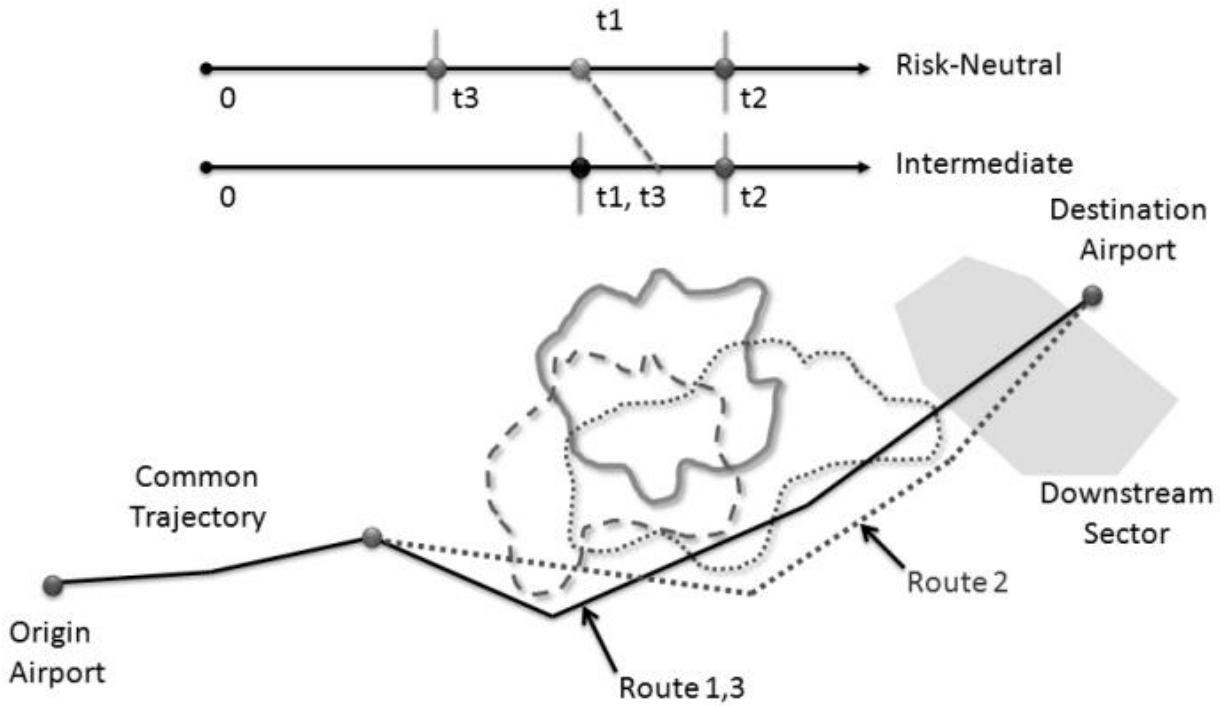

Figure 4. Intermediate Strategy Resulting in Larger Delays and Smaller Variation

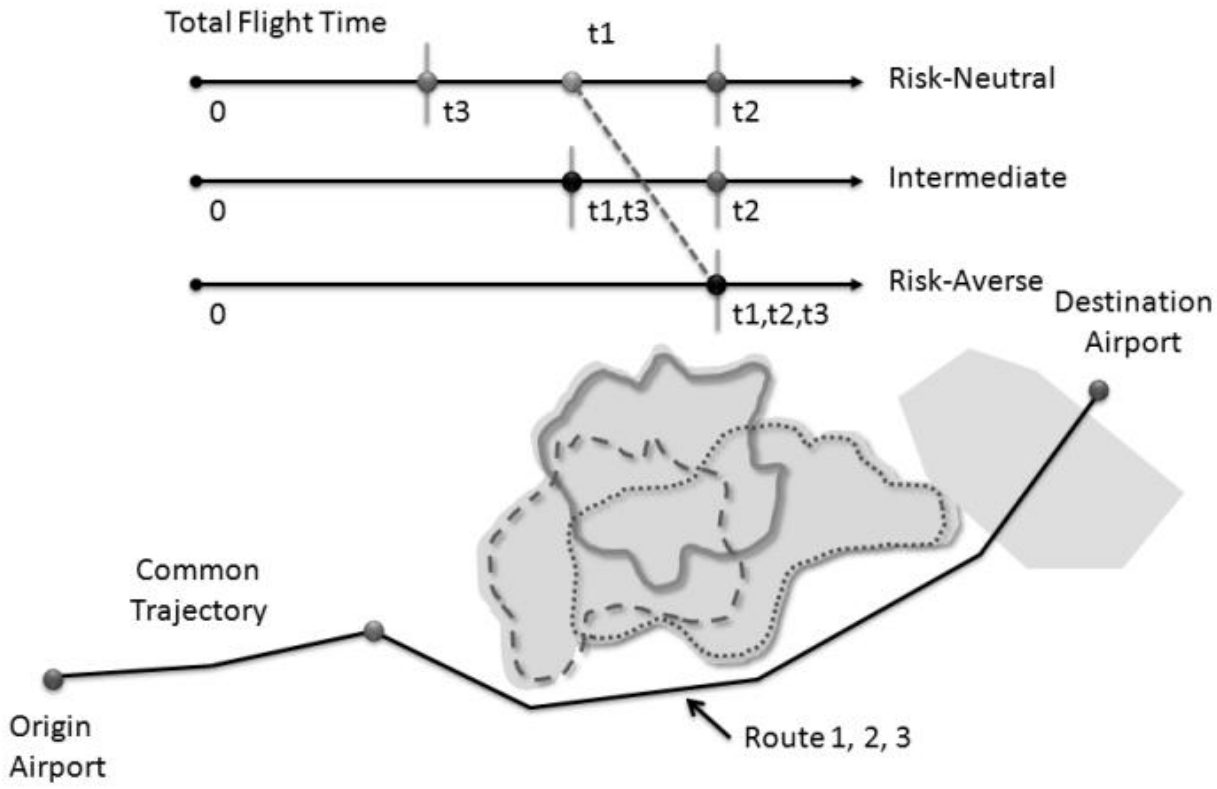

Figure 5. Risk-Averse Trajectory with No Variation

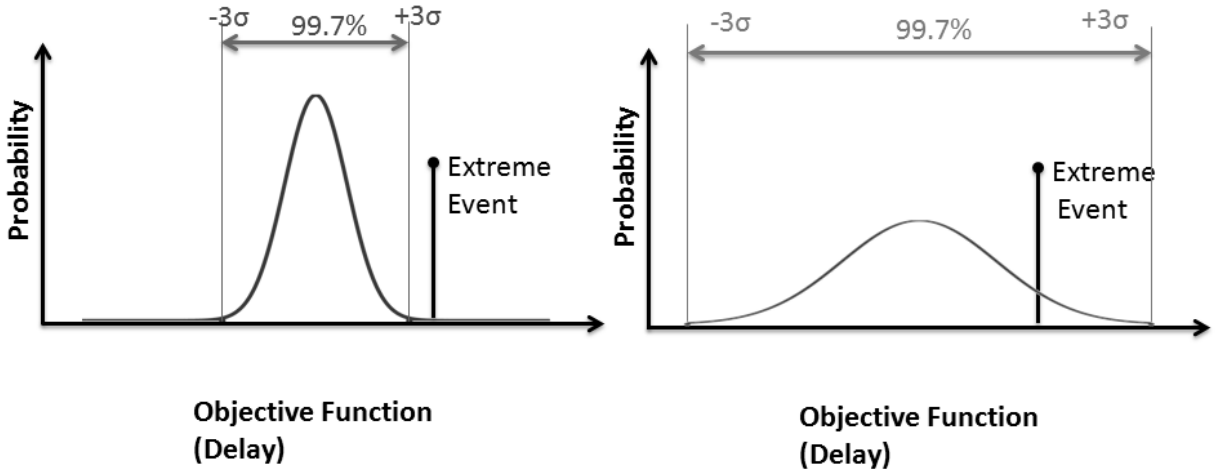

Figure 6. Spread of a Probability Distribution as a Measure of Risk

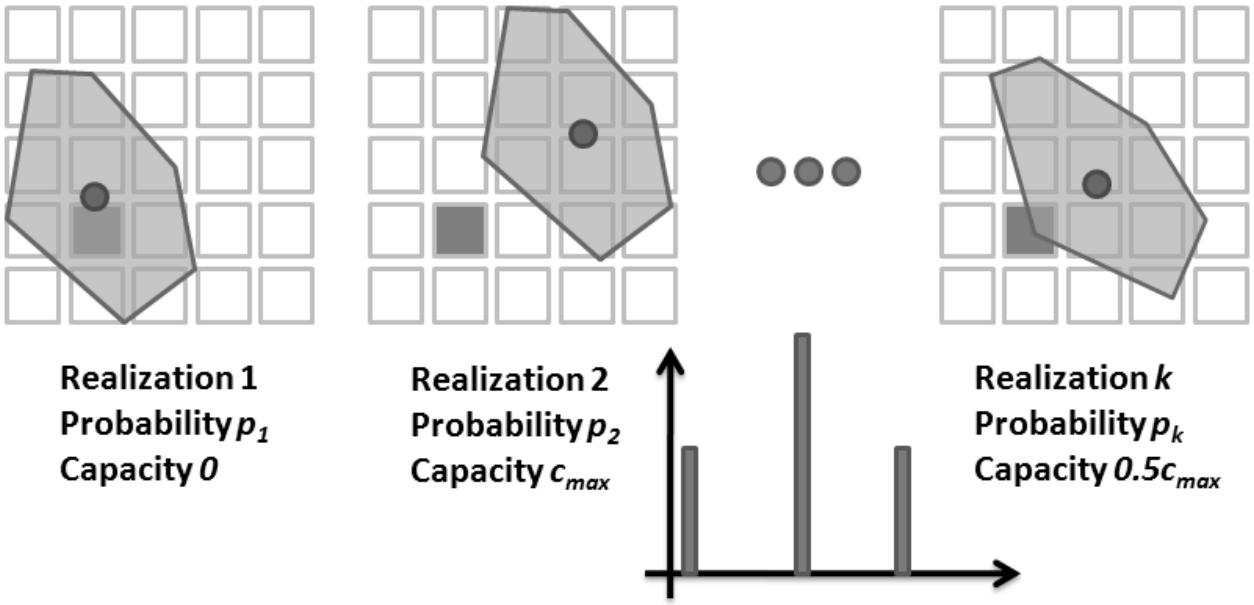

Figure 7. Effect of Weather on Sector Capacities

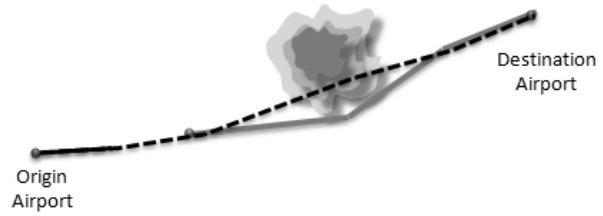

(a) Avoidance of the Mean of All Weather Realizations

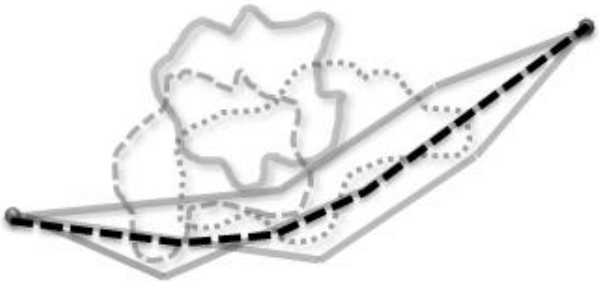

(b) Flying on the Mean of All Possible Reroutes

(c) "Risk-Averse" Trajectory

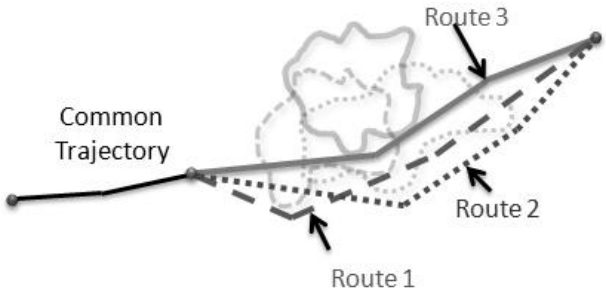

(d) "Risk-Neutral" Trajectory

Figure 8. Strategies for Risk Management

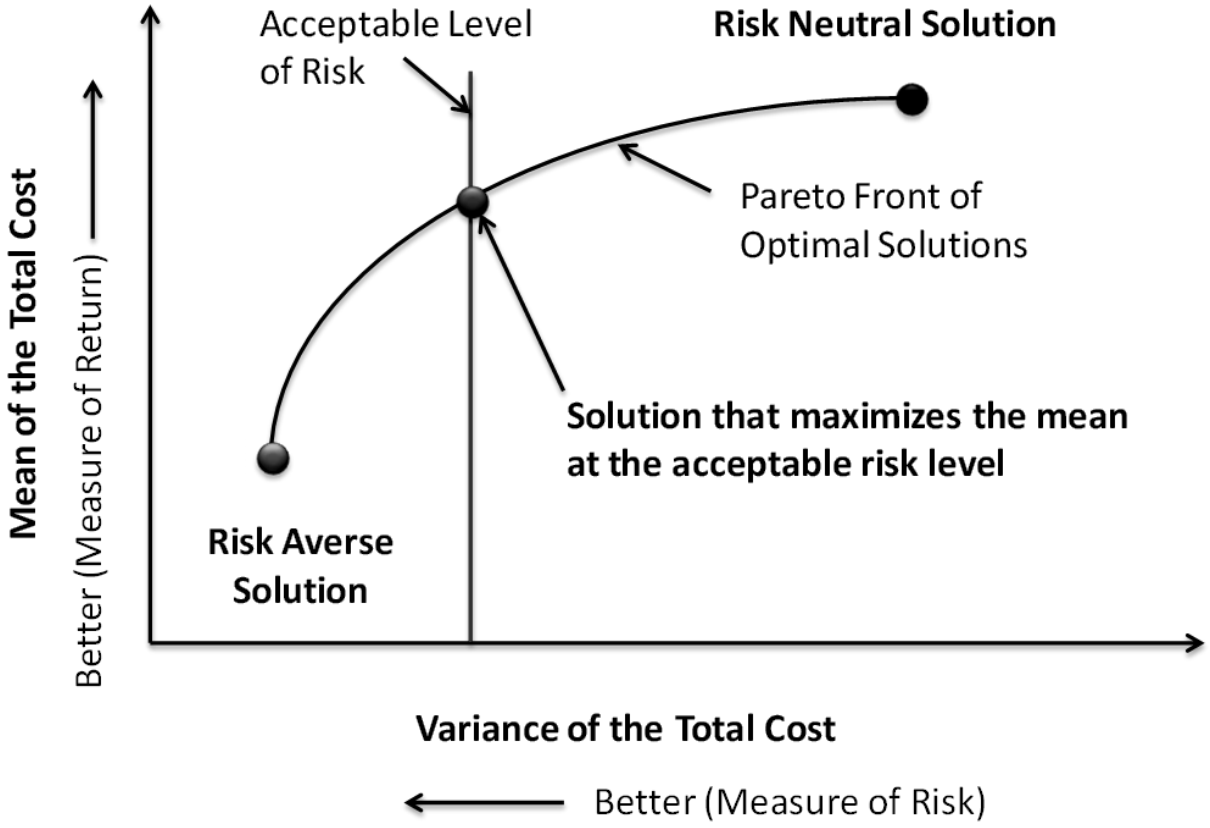

Figure 9. Mean-Variance Tradeoff

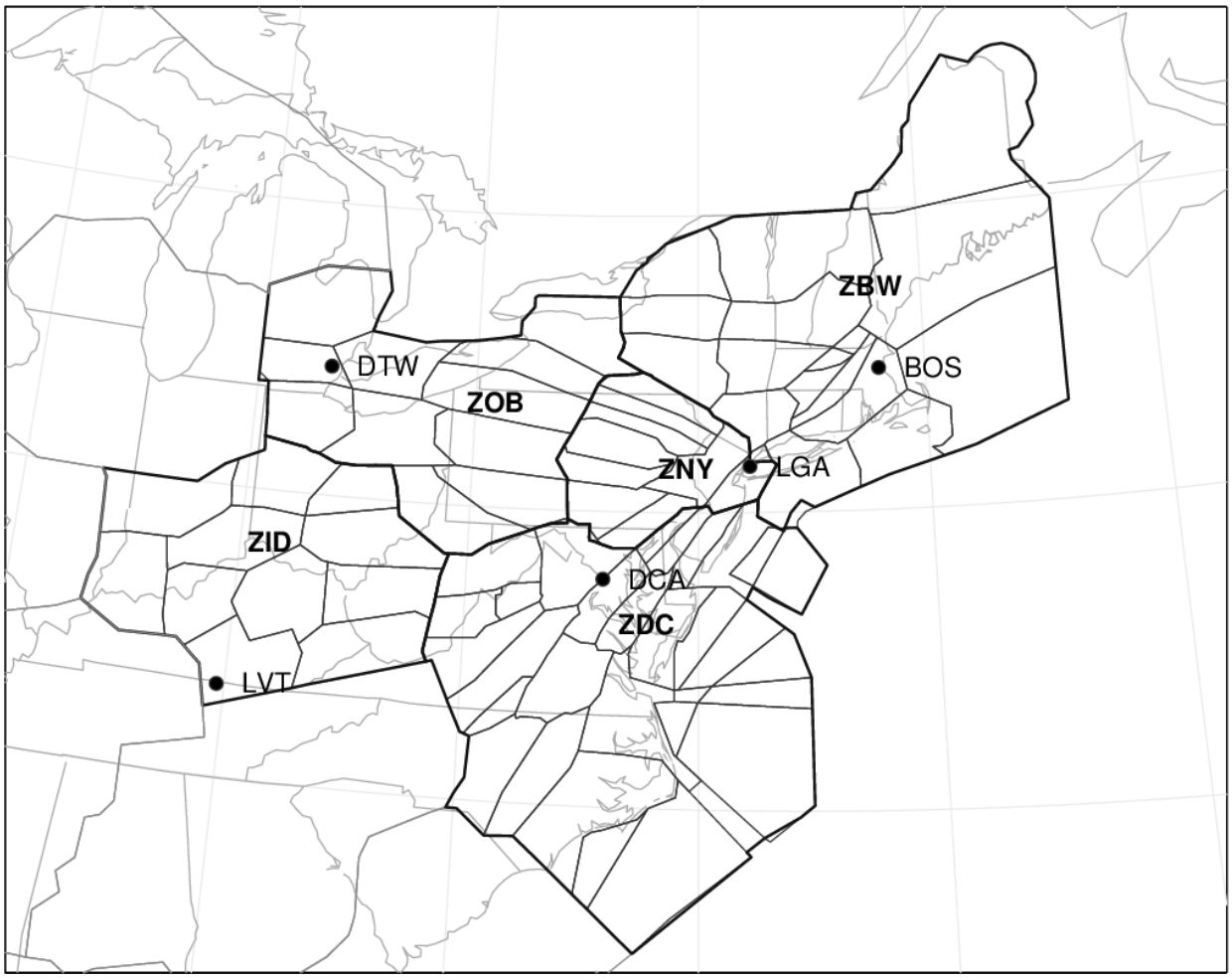

Figure 10. The Region of Interest

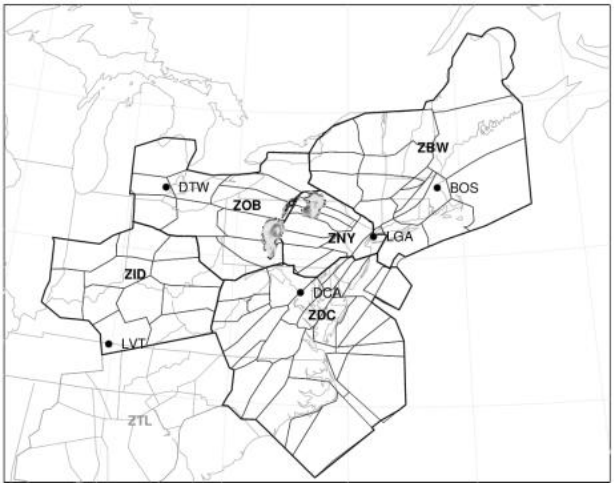

(a) Scenario 1

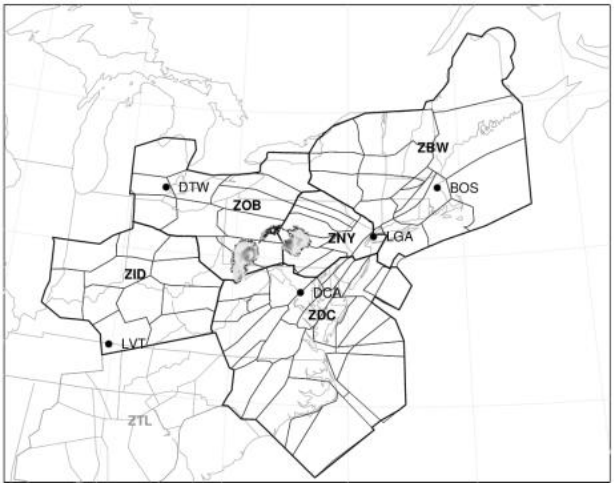

(b) Scenario 2

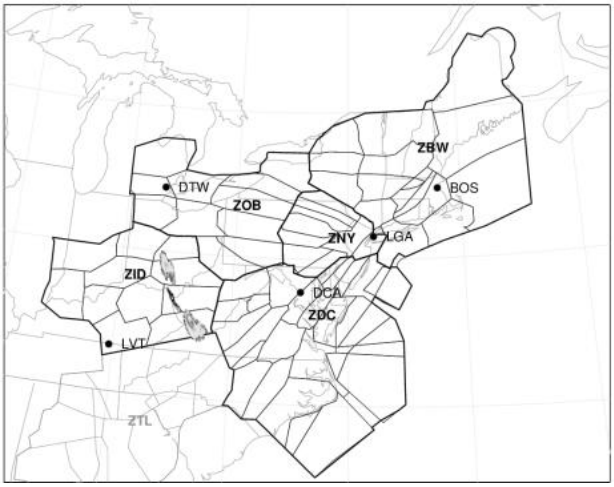

(c) Scenario 3

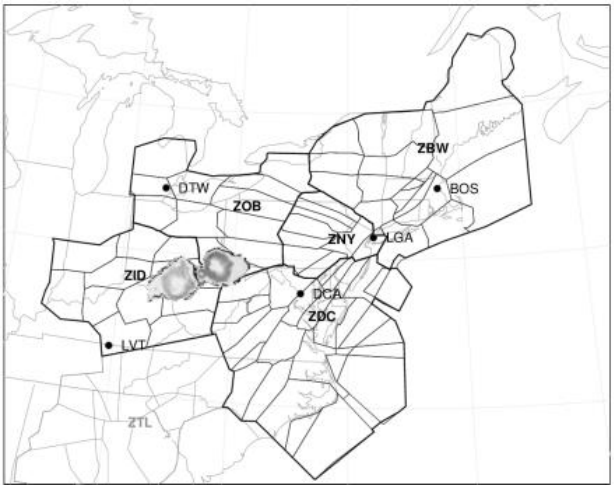

(d) Scenario 4

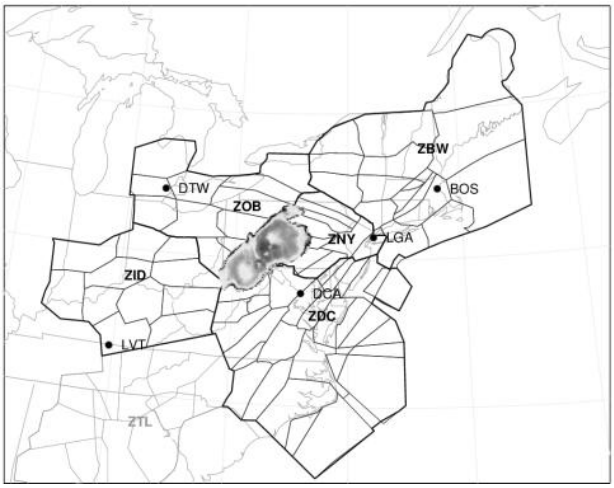

(e) Scenario 5

Figure 11. Stochastic Weather Realizations

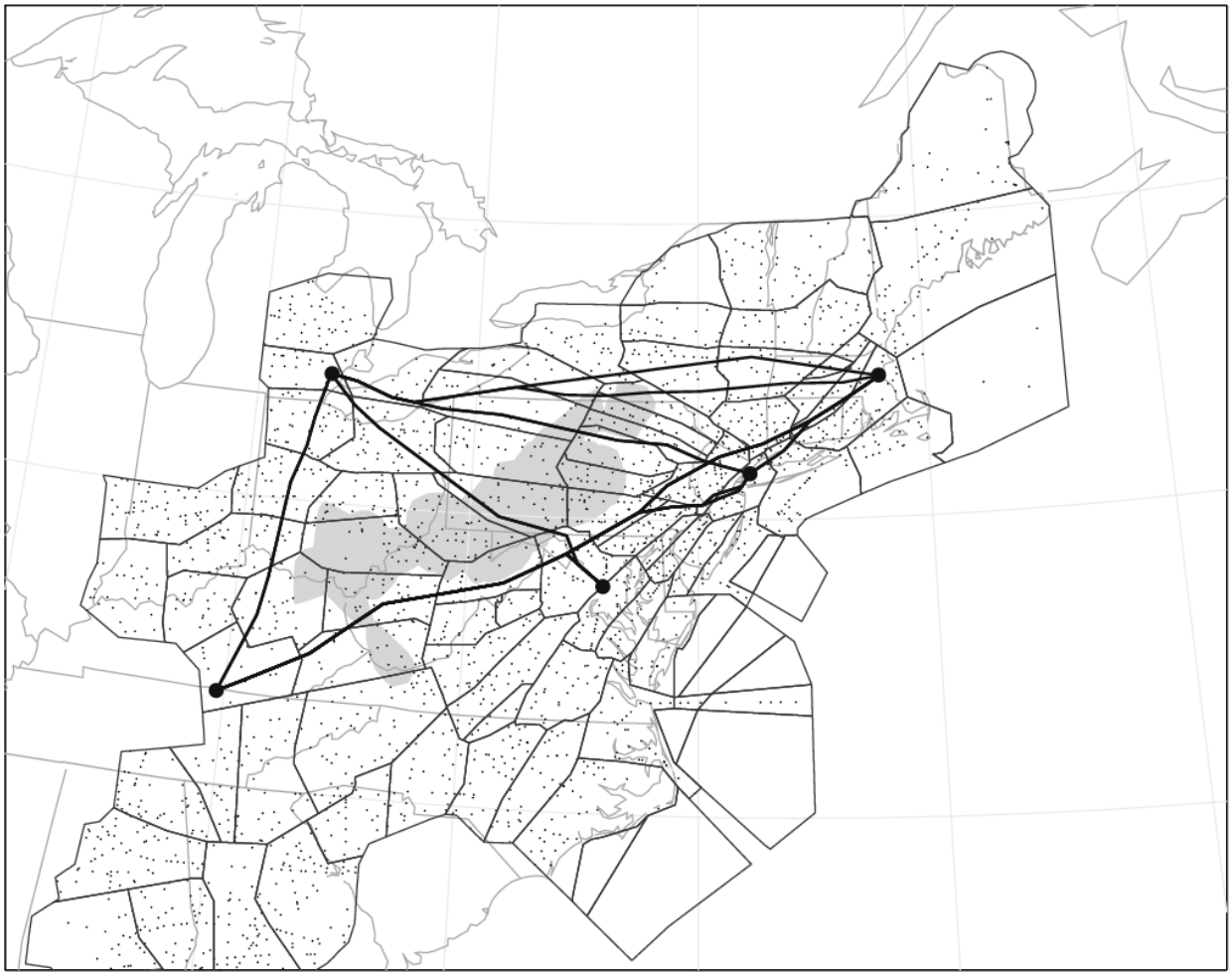

Figure 12. Nominal Routes between Airports

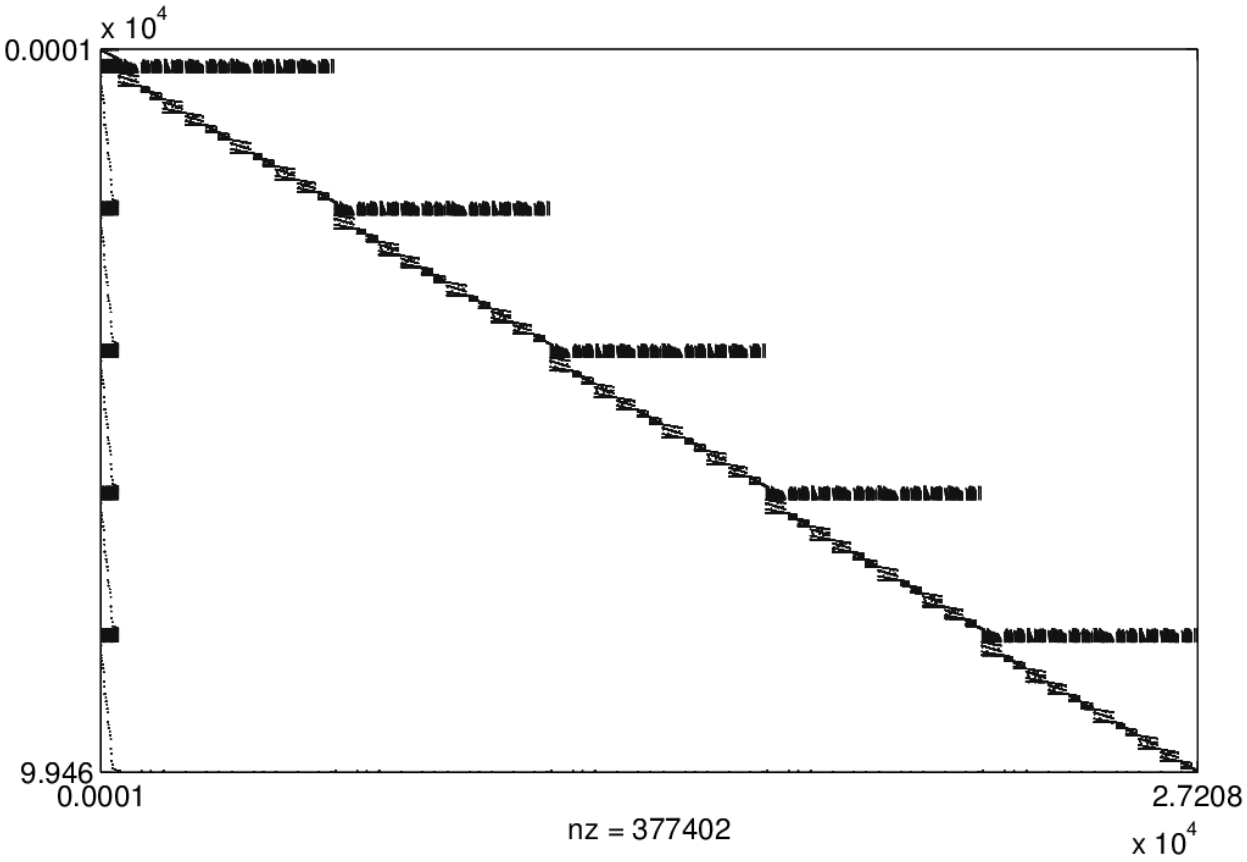

Figure 13. Constraint Matrix Structure for 5 Scenarios with 15 Flights

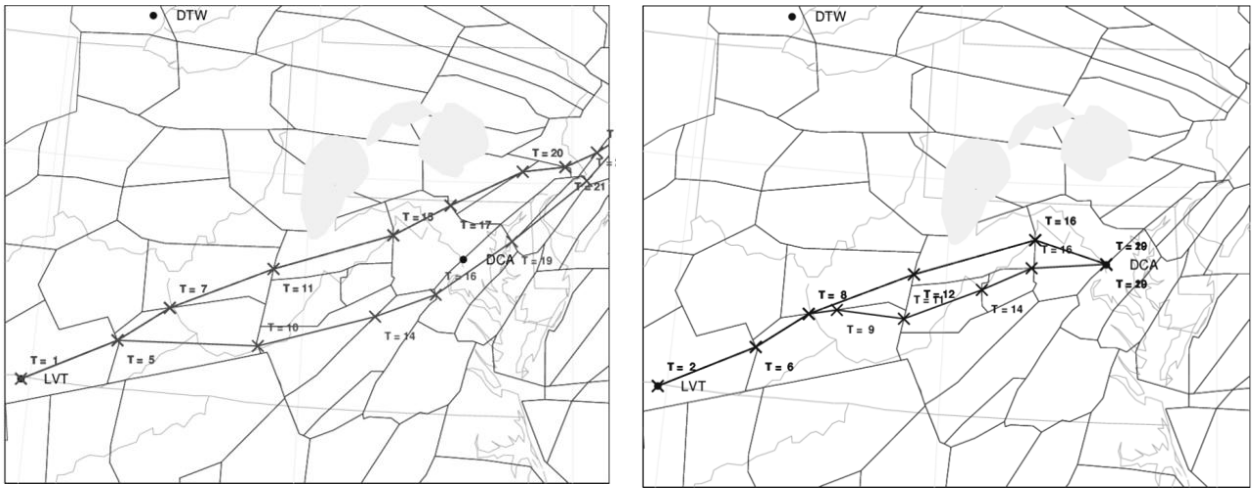

(a) Destination LGA **(b) Destination DCA**

Figure 14. Ground Stop at LVT

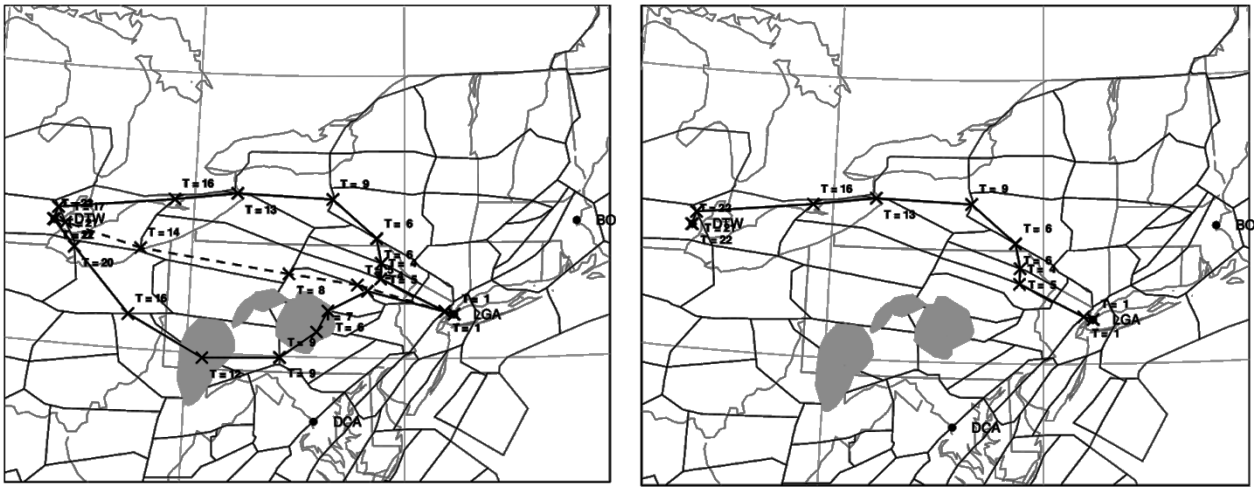

(a) Risk-Neutral Strategies for each Weather Realization **(b) Risk-Averse Strategy**

Figure 15. Risk-Neutral vs. Risk-Averse Strategy from LGA to DTW

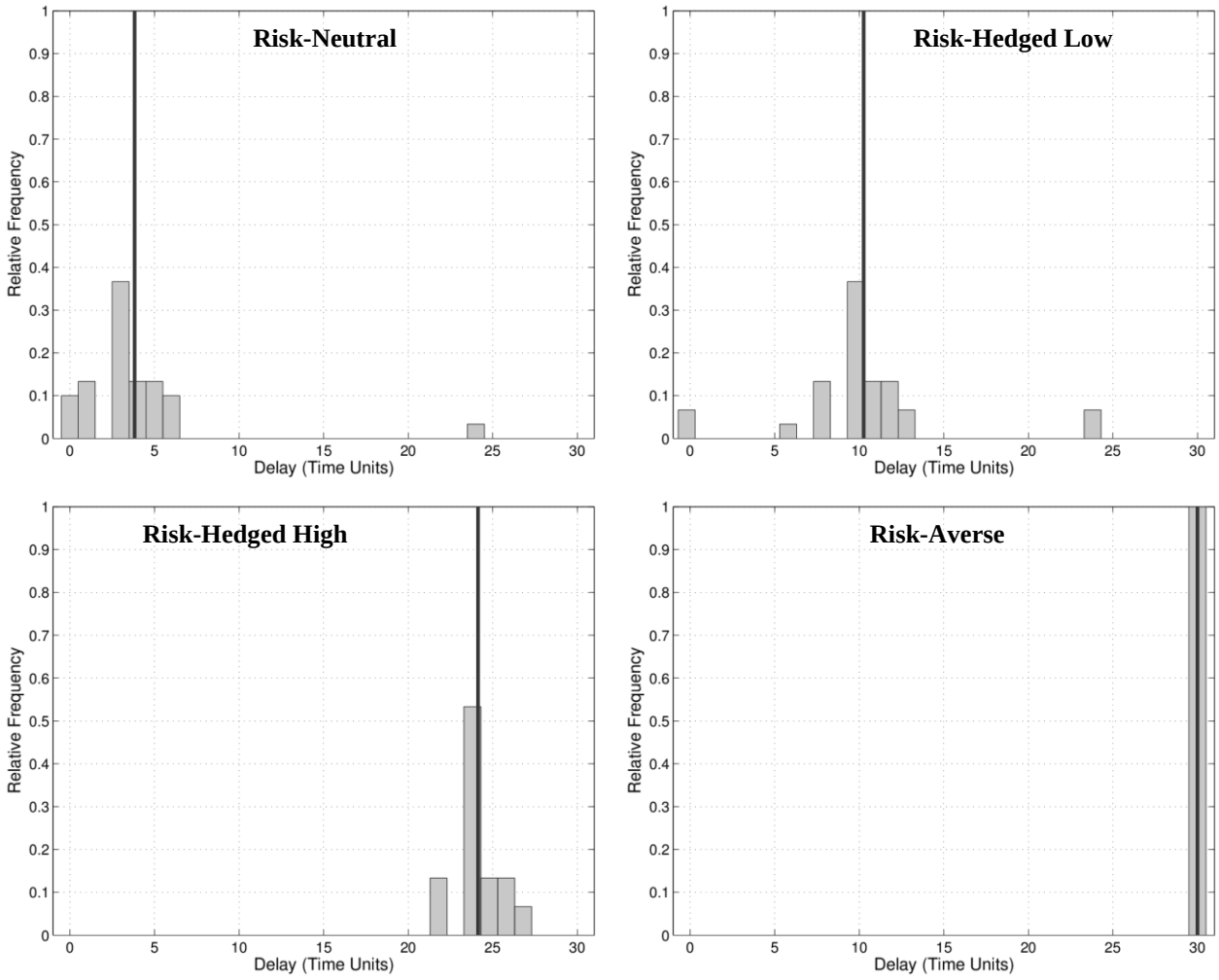

Figure 16. Relative Frequency Histogram of Deviations from Mean Delay for $\alpha = 1.00, \alpha = 0.67, \alpha = 0.13, \alpha = 0.00$

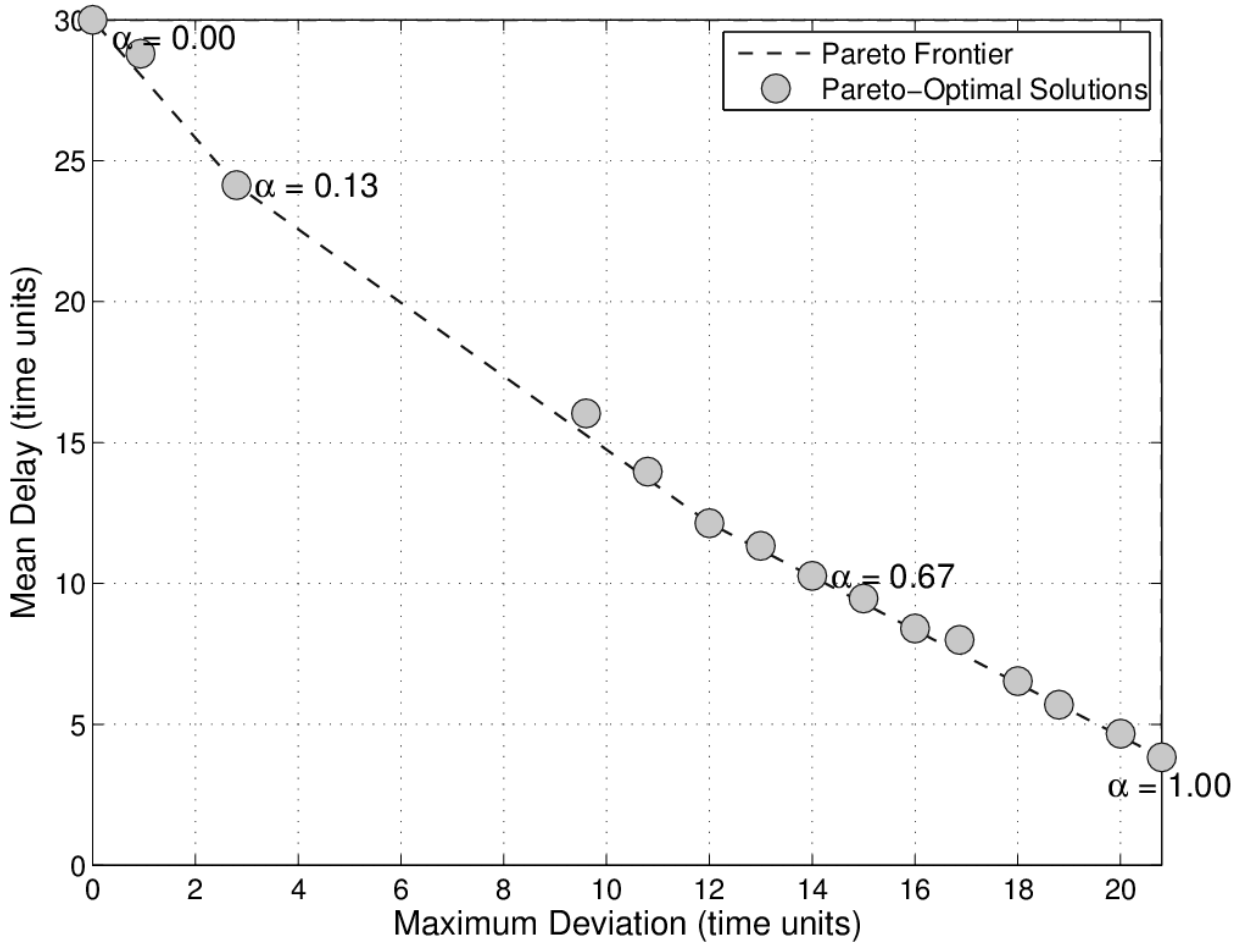

Figure 17. Pareto-Optimal Solutions for Trade-Off between Mean Delay and Maximum Deviation from Mean Delay